농학석사학위논문

Pentachlorophenol의 제브라피쉬 성체에서 대사체학 및 단백질체학을 통한 독성학적 해석

Toxicological interpretation of pentachlorophenol through metabolomic and proteomic analysis in adult zebrafish

2021년 2월

서울대학교 대학원

농생명공학부 응용생명화학전공

한 희 주

A Dissertation for the Degree of Master of Science

Toxicological interpretation of pentachlorophenol through metabolomic and proteomic analysis in adult zebrafish

February 2021

Heeju Han
Applied Life Chemistry Major
Department of Agricultural Biotechnology
Seoul National University

Pentachlorophenol의 제브라피쉬 성체에서 대사체학 및 단백질체학을 통한 독성학적 해석

Toxicological interpretation of pentachlorophenol through metabolomic and proteomic analysis in adult zebrafish

지도교수 김 정 한

이 논문을 농학석사학위논문으로 제출함

2020년 12월

서울대학교 대학원

농생명공학부 응용생명화학전공

한 희 주

한희주의 석사학위논문을 인준함

2021년 1월

위 원 장 _____ 이 상 기 _____ (인)

부 위 원 장 _____ 김 정 한 _____ (인)

위 원 _____ 김 민 균 _____ (인)

Abstract

Pentachlorophenol (PCP) has been used as an insecticide and wood preservative, and classified as a carcinogenic grade 2B. Since PCP could be exposed to aquatic organisms through the environment contamination due to its high chemical stability, the toxic mechanisms of PCP in adult zebra fish was investigated using targeted metabolomics with GC-MS/MS and proteomics with LC-orbitrap-MS/MS. Zebra fish was exposed to PCP in three groups including control, low exposure group (1/10 LC_{50}) and high exposure group (LC_{50}) for 48 h. In the case of GC-MS/MS, 397 individual metabolites were analyzed on multiple reaction monitoring mode to identify 180 metabolites. Statistical analysis was performed with SIMCA+ and Metaboanalyst 4.0. Three groups were well separated on principal component analysis (PCA) or partial least squares-discriminant analysis (PLS-DA), and 74 metabolites were selected as biomarkers through variable importance in the projection (VIP) and analysis of variance (ANOVA) tests to construct heat map. Oxidative stress caused by PCP was also confirmed through MDA and ROS assay. Eight metabolic pathways were observed to show toxicologically significant alteration. Proteomics was performed with control and high exposure group to identify 2108 proteins, of which 376 proteomic biomarkers were selected through fold change screening. Gene ontology (GO) analysis of those proteomic biomarkers revealed protein expression level in biological process, molecular function and cellular components were altered. Integrated metabolic pathways of metabolomic/proteomic perturbation were proposed including pentose phosphate pathway, pentose and glucuronate interconversions, phenylalanine metabolism, ascorbate and aldarate metabolism, taurine and hypotaurine metabolism, alanine, aspartate and glutamate metabolism and β-alanine metabolism. Such perturbation

of metabolomics/proteomic pathway in zebrafish by PCP results in significant toxicological effects and activation of defense mechanisms.

Key words: Metabolomics; Proteomics; Pentachlorophenol; Zebrafish; GC-MS/MS; LC-MS/MS

***Student Number*: 2019-23867**

Table of Contents

List of Tables

List of Figures

Introduction

Pentachlorophenol (PCP) is an organochloride pesticide, which has been used worldwide as a wood preservative and insecticide (Ware, 2000; Lin, 2000). PCP structure has stable aromatic ring and high chlorine content, so it is prone to be persistent in the environment. PCP was designated as Endocrine Disrupting Chemicals (EDCs) and persistent organic pollutants (POPs) (EPA, 2008; United Nations, 2010), and even was classified as a group 2B carcinogen by IARC (IARC, 1991).

Although the use of PCP has been restricted since the 2000s, cases of exposure are still being reported in various environments. In 2008, the estimated amount of PCP released in the USA was 172 kg, 513 kg, and 1865 kg to air, water and landfills, respectively (Lin, 2000). PCP has been detected in drinking water, river water, house-hold dust, and even breast milk (Hong et al., 2005; Ward et al., 2009; Michałowicz et al., 2011; Zheng et al., 2012). Moreover, PCP accumulations of aquatic organisms have been found in several reports (Basheer et al., 2004; Ge et al., 2007). Therefore, it is important to investigate the toxicological effect of PCP exposure in aquatic organisms. Among the aquatic organisms, zebrafish has been used in many toxicology studies (Peterson and MacRae, 2012; Dai et al., 2014) because it is known to be homologous to mammals physiologically and genetically (Mishra et al., 2017), and approximately 86 % of human drug targets have been identified in zebrafish (Gunnarsson et al., 2008).

Recently, omics techniques have been widely used to uncover pathological change and identify potential disease markers (Chen et al., 2020). Metabolomics is one of the emerging omics tools for elucidating metabolic alterations in organisms under a given set of conditions through analysis of large amount of various metabolomes in biological samples (Ibero-Baraibar et al., 2016). Toxicometabolomics focuses on metabolomics interpretation for toxicological effect of toxicants on Biosystems (Krieger et al., 2010). The popular methods for

metabolomics include gas chromatography/mass spectrometry (GC/MS), liquid chromatography/mass spectrometry (LC/MS), and nuclear magnetic resonance (NMR) (Kuehnbaum et al., 2013). Although NMR provides rapid metabolome analysis, it has general limit of the number of metabolites due to overlapping of peaks while MS is more sensitive and selective in detecting abundance metabolites (Zamboni et al., 2015; Wang et al., 2018). In addition to metabolomics, proteomics provides promising diagnostic and prognostic information through identifications and integrative analysis at the protein level (Navas-Carrillo et al., 2017). And in proteomics, the approaches using mass spectrometry (MS) have been developed to identify all proteins of a cellular proteome with higher sensitivity (Yates III, 2011). Toxicoproteomics also deals with elucidation of proteomic changes by toxicological alteration of biosystems through its exposure to toxic agents (Krieger, 2010). The omics cascade (Figure 1) indicates that integrative interpretation of metabolomics and proteomics could link the changes in genotype and phenotype (MacMullan et al., 2019). Therefore, interpretation of metabolomics' results by integration with proteomics' data will provides more confirmative, comprehensive and integrative understanding of metabolic/proteomic pathways which are perturbed by toxicological phenomenon (Villar et al., 2015; Song et al., 2017).

In this study, PCP was exposed to zebrafish at two different concentrations and the 397 metabolomes were analyzed on targeted mode on GC-MS/MS to find out biomarker metabolomes. Statistical analysis such as PCA, PLSDA, VIP, ANOVA and heat map and identification of metabolic pathways was performed with SIMCA^{+} or Metaboanalyst 4.0. In proteomics, pooled zebrafish sample was analyzed on LC-orbitrap-MS/MS to screen biomarker proteomes and ontology investigation. The metabolic pathways were identified first by biomarker metabolomes and then, by integration of metabolomics' results and proteomics data to characterize the toxicologically and biochemically altered metabolomic and proteomic physiology.

Figure 1. **The Omics cascade.** It follows from genotype to phenotype with genomics, transcriptomics, proteomics and metabolomics.

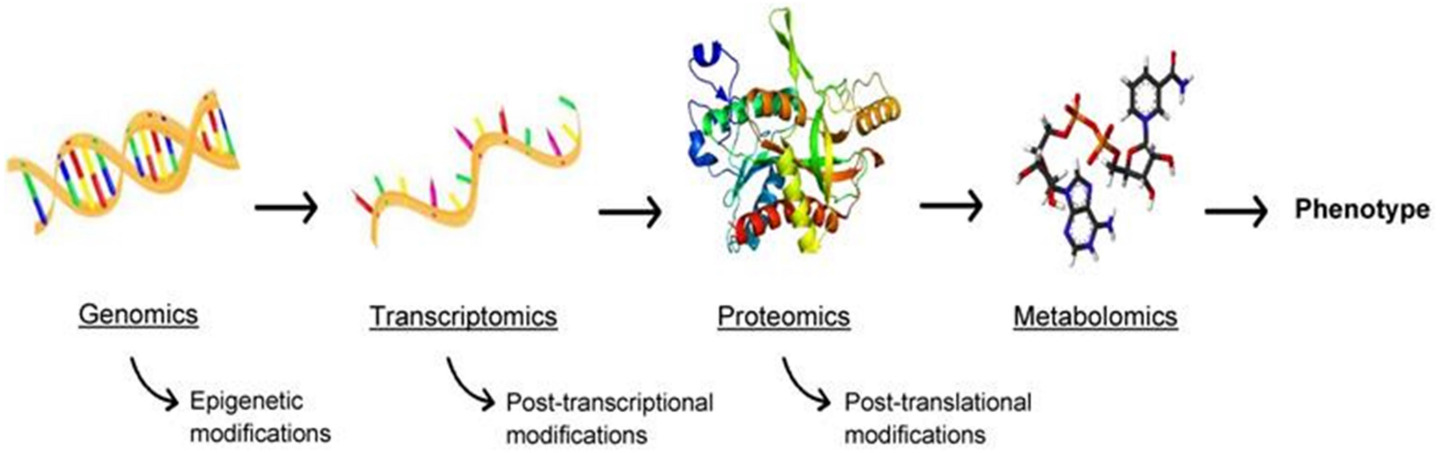
Genomics
Transcriptomics
Proteomics
Metabolomics
Phenotype
Epigenetic modifications
Post-transcriptional modifications
Post-translational modifications

Materials and Methods

Chemicals and reagents

Pentachlorophenol was purchased from AccuStandard, and ribitol as an internal standard was from Wako. 1 % TMCS-MSTFA reagent was purchased from Thermo Fisher Scientific Company. Methoxyamine hydrochloride, N,N-dimethylformamide (DMF), methanol (MeOH), dimethyl sulfoxide (DMSO) and pyridine were purchased from Sigma-Aldrich. Ammonium bicarbonate, urea, iodoacetamide, DL-dithiothreitol (Sigma–Aldrich) were used as ≥ 99%. Sequencing grade modified trypsin was obtained from Promega Corporation. Sep-Pak C18 cartridge was obtained from Waters Corporation (1 cc, 100 mg). Acetonitrile and water were of liquid chromatography-mass spectrometry grade and purchased from Fisher Scientific. The highest available grade products were used for every reagent. Methoxyamination reagent was prepared by dissolving 20 mg methoxyamine hydrochloride in 1 mL of pyridine

Experimental animals and exposure to PCP

Adult zebrafish were acclimated at 26 ± 1 °C in a glass water tank for 2 weeks. The photoperiod was maintained as a 16:8 h light:dark cycle. During this period zebrafish were fed with a commercial fish feed, and they were not fed the day before PCP exposure. The LC_{50} value of PCP for zebrafish is 130 μg /L for 48 hour, sustaining up to 96 hour (Yin et al., 2006). Based on this value, the exposure concentration was set at 130 μg/L and 13 μg/L for the high exposure and low exposure group, respectively.

In 10 L beaker, 30 zebrafish per each group were kept before exposing to 130 μg/L (high exposure; LC_{50}) and 13 μg/L (low exposure; 1/10 LC_{50}), including of control group without PCP, for 48 h. After exposure, 6 zebrafish were sampled in

each group for metabolomes and oxidative stress analyses. During the experiment, the exposure solution was changed daily to maintain the PCP concentration.

Metabolomic sample preparation, profiling and metabolomes identification by GC-MS/MS).

Using a mortar and pestle, fish samples frozen by liquid N_2 were ground into a fine powder. One mL of 50 % MeOH solution containing 0.2 μg/mL of ribitol (internal standard) was added to a 50 mg of ground sample, and then the sample was vortexed at 4 °C for 10 min. After centrifuging the extracts for 10 min at 13,000 rpm, 100 μL of supernatant of the extracts was evaporated by a speed vacuum concentrator (Hanil Modulspin 40). The dried residue was reacted with 50 μL of methoxyamination reagent for 90 min at 37 °C with shaking, and then derivatized with 50 μL of MSTFA reagent (MSTFA + 1 % TMCS) for 30 min at 37 °C.

For analysis of metabolites, Shimadzu GCMS-TQ8040 equipped with BPX-5 column (30 m ×0.25 mm i.d., 0.25 μm film thickness, TRAJAN) was used with MRM mode for a total of 397 metabolites (331 metabolites from the Smart Metabolites Database, and 66 metabolites from in-house library). Injection volume was 1.0 μL (Split mode; 30:1) and temperature for injector, transfer lines and ion source (70 eV) were 250 °C ,280 °C and 200 °C, respectively. The oven temperature was started at 60 °C (2 min), and the temperature was increased to 320 °C at a rate of 10 °C/min and maintained for 15 min. Argon was used for the collision gas and helium was used for carrier gas with a flow rate was 1 mL/min. Data processing was performed with manual reconfirmation of the peak detection using GCMS Solution software (version 4.3, Shimadzu). The relative area of individual metabolites was calculated by comparing peak areas of the metabolites and the internal standard (ribitol).

Statistical analysis of metabolomes and metabolic pathway analysis

The multivariate data analyses were conducted using SIMCA-P $^{+}$ software (version 12.0.1, Umetrics, Sweden). Principal component analysis (PCA) was carried out to calculate the value of accumulated variance contribution rate (R^2X). The supervised multidimensional statistical model, a partial least squares-discriminant analysis (PLS-DA), was performed to distinguish between each treatment group, confirming with the R^2Y and Q^2 values. The VIP (variable importance in the projection) in PLS-DA was calculated to select metabolites with VIP scores > 1 and standard errors < 1. After those metabolites were analyzed using a one-way ANOVA, p-value was calculated to select the biomarker metabolites that were significantly affected by exposure to PCP ($p < 0.05$). A heat map was generated with MetaboAnalyst 4.0 (www.metaboanalyst.ca) using those biomarker metabolites that had been selected through the VIP and ANOVA. Metabolic pathway analysis plots were produced with MetaboAnalyst 4.0 based on the Danio rerio KEGG library.

Proteomic sample preparation, profiling and identification of proteomes by LC-Orbitrap-MS/MS

A 4mg of the ground powder from 6 individuals of control and exposed groups were pooled and homogenized in 500 μL of 0.1M phosphate buffer (pH7.4), before filtering with cell strainer and then centrifuged at 1,000g at 4°C for 20 min. The protein concentrations of supernatant were determined according to the Bradford method (Quick Start™ Bradford Protein Assay Kit, Bio-Rad, Inc., CA, USA). The absorbance was detected at 595 nm using a spectrophotometer (Spectra Max i3, Molecular Devices Co.,CA, USA). A 200 μg equivalent of protein in the supernatant was evaporated, and the proteins were with 30.0 μL of 6 M urea in 50 mM ammonium bicarbonate for 3 h at room temperature. The solution was treated with 100 mM dithiothreitol (3.0 μL) and incubated for 3 h at room temperature,

and further treated with 100 mM dithiothreitol (6.8 µL), 0.55 M iodoacetamide (1.2 µL) and incubated for 1 h under dark conditions. The sample was diluted with 164.2 µL of 50 mM ammonium bicarbonate, and treated with 4 µg trypsin in 40 µL buffer, followed by shaking for 18 h at 37℃. The digested protein solution was acidified by adding 9.8 µL of 10% formic acid. A Sep-Pak C18 cartridge was conditioned with 5 mL of Solvent A (0.1% formic acid in 2% acetonitrile) and then 10 mL of Solvent B (0.1% formic acid in 65% acetonitrile). The digested protein solution was loaded onto the cartridge, washed with 10 mL of Solvent A and eluted with 1 mL of Solvent B twice. The eluate was dried in a speed-vacuum concentrator and reconstituted in 50 µL of Solvent A.

A 3 µL of aliquot was injected into an ultra-high-performance liquid chromatography (UHPLC, Dionex UltiMate 3000) equipped with an Acclaim PepMap 100 trap column (100 µm x 2 cm, nanoViper C18, 5 µm, 100 Å) and subsequently washed with 98% Solvent A for 10 min at a flow rate for 4 µL/min. The sample was continuously separated on a PepMap RSLC capillary column (75 µm x 50 cm, C18, 2 µm, 100 Å) at a flow rate of 300 nL/min with water in 0.1% formic acid (A) and acetonitrile in 0.1% formic acid (B) as the mobile phases (all v/v). The following gradient was used: 5% B for 0-5 min, 5 to 10% B for 5-10 min, 10 to 40% B for 10-150 min, 40 to 95% B for 150-152 min, 95% B for 152-162 min, 95 to 5% B for 162-165 min and 5% B for 165-180 min. Peptide samples were ionized on ESI mode of QExactive Orbitrap HRMS (Thermo Fisher Scientific, USA) through a coated silica-emitted tip (PicoTip emitter, New Objective, USA) at an ion spray voltage of 2200 eV. The MS spectra were acquired at a resolution of 70,000 in a mass range of 350-1,800 m/z, and the MS/MS spectra were measured in a data-dependent mode at a resolution of 17,500. MS spectral data were obtained using Xcalibur software (Thermo Fisher Scientific Inc.) and the proteins were identified using Proteome Discoverer 2.4 (PD 2.4, Thermo Fisher Scientific Inc.)

with selected Danio rerio FASTA database from National Center for Biotechnology Information (NCBI).

Proteome biomarkers and gene ontology

Those identified proteins on LC-Orbitrap-MS/MS were evaluated by p-value (T-test; < 0.05) and fold change (< 0.5 or > 2.0) to select proteome biomarkers that significantly contributed to distinguish proteomic profiles between two groups). Each number of down regulation (fold change <0.5) and up regulation (fold change > 2.0) was calculated. Gene ontology (GO) analysis of WebGestalt was conducted with proteome biomarkers to identify various genes in biological process, molecular function and cellular components.

Integrative metabolomics and proteomic pathways

Integrative metabolomics and proteomic pathways were generated using integrative pathway analysis of MetaboAnalyst 4.0. Each selective pathway was interpreted based on metabolomes/proteomes changes and concepts from KEGG map

Measurement of ROS and MDA contents

The reactive oxygen species (ROS) content was determined using DCFH-DiOxyQ (OxiSelect^{TM} In vitro ROS/RNS assay kit, Cell Biolabs, Inc., CA, USA). A 20 mg of sample powder was homogenized in 500 μL of phosphate buffered saline (PBS), and the homogenates were centrifuged at 10,000g for 5 min. A 50 μL of the supernatant was mixed with 50 μL of catalyst and incubated for 5 min at room temperature. The DCFH solution 100 μL was added into the mixture and incubated at room temperature for 40 min. The fluorescence was measured at 480 nm excitation / 530 nm emission using a spectrophotometer (SpectraMax i3, Molecular Devices).

The quantitative determination of malondialdehyde (MDA) was performed using thiobarbituric acid (TBA) assay (OxiSelect™ TBARS assay kit, Cell Biolabs, Inc., CA, USA). A 30 mg of sample powder was homogenized in 500 μL of 1X butylated hydroxytoluene (BHT) solution, and the homogenates were centrifuged at 10,000g for 5 min. A 100 μL of the supernatant was mixed with 100 μL of SDS Lysis solution and incubated for 5 min at room temperature. The TBA reagent 250 μL was added into the mixture and incubated at 95℃ for 60 min. After incubation, sample tubes were cooled to room temperature and centrifuged at 3000 rpm for 15 min. The supernatant (300 μL) was extracted with butanol (300 μL) to prevent the interference of hemoglobin and its derivatives. The fluorescence of butanol solution was measured at 540 nm excitation / 590 nm emission using a spectrophotometer (SpectraMax i3, Molecular Devices).

Results and Discussion

Metabolome profiling/identification

Modern GC-MS/MS offers the sensitive, selective and simultaneous analysis of large number of metabolomes by employing the targeted MRM mode (Hirata et al., 2017; Zaitsu et al., 2019). Thanks to its advantages compared to non-targeted methodology, targeted metabolomics plays important roles in medical and toxicology arenas (Tsugawa et al., 2014; Hirata et al., 2017; Zaitsu et al., 2018). For targeted metabolomics in this study, a total of 397 metabolites (331 metabolites from the Smart Metabolites Database, and 66 metabolites from in-house library) of 102 organic acids, 78 carbohydrates, 75 amino acids, 41 fatty acids, 18 alcohols, 11 nucleosides, 11 purines, 10 amides, 10 amines, 9 phenols, 7 pyridines, 6 steroids, 4 pyrimidines, 4 indoles, 3 esters, 2 terpenes, 2 tocopherols, 1 azole, 1 glyceride, 1 inorganic compound and 1 phosphoric acid were analyzed using GC-MS/MS and 180 metabolites were identified (Figure 2, Table 1). These identified metabolites consisted of 44 carbohydrates, 40 organic acids, 38 amino acids, 16 fatty acids, 9 purines, 7 alcohols, 6 amides, 4 amines, 3 pyrimidines, 2 esters, 2 indoles, 2 phenols, 2 steroids, 1 inorganic compound, 1 nucleoside, 1 phosphoric acid, 1 pyridine and 1 tocopherol.

Figure. 2. TIC of metabolites in whole-body zebrafish samples under high-concentration (130 μg/L) of PCP exposure conditions (A) and individual chromatograms of some metabolites and the ribitol internal standard (B).

(A)

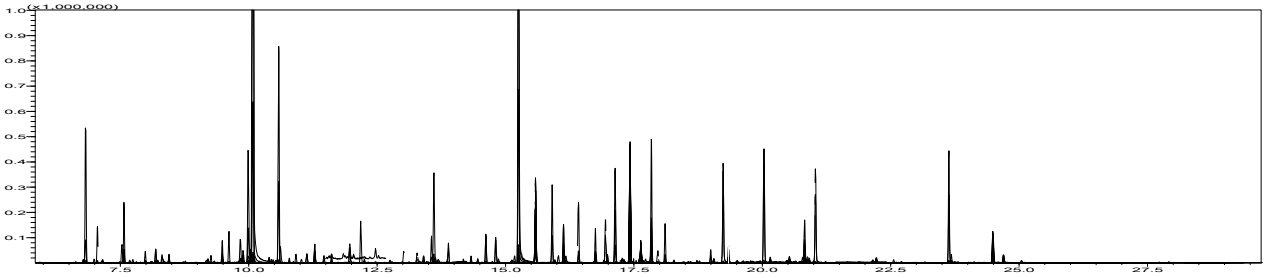

(B)

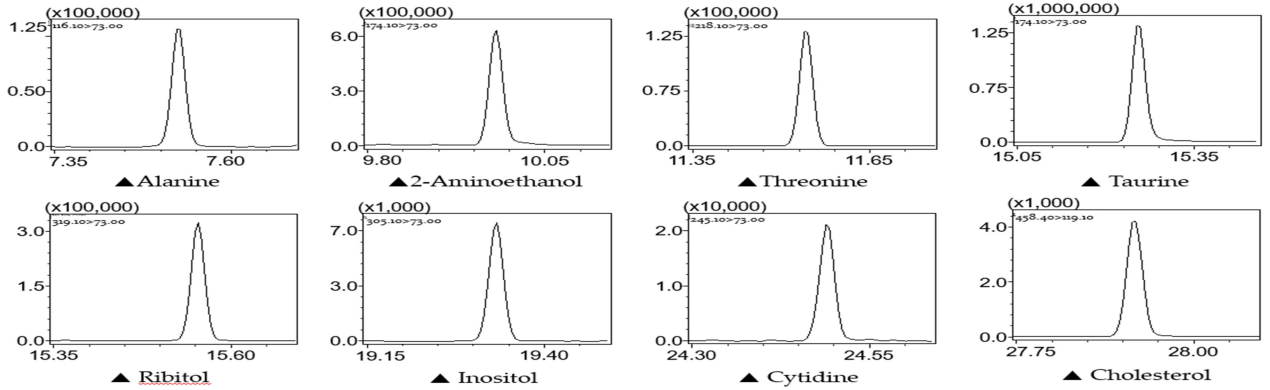
(x100,000)
116.10>73.00
Alanine
(x100,000)
174.10>73.00
2-Aminoethanol
(x100,000)
218.10>73.00
Threonine
(x1,000,000)
174.10>73.00
Taurine
(x100,000)
319.10>73.00
Ribitol
(x1,000)
305.10>73.00
Inositol
(x10,000)
245.10>73.00
Cytidine
(x1,000)
458.40>119.10
Cholesterol

Table 1. Metabolites detected in whole-body zebrafish samples by targeted metabolite analyses using GC-MS/MS with MRM mode.

Class	No	Metabolites	Class	No	Metabolites	Class	No	Metabolites
alcohols	1	1-Hexadecanol	amino acids	20	2-Aminoisobutyric acid	amino acids	39	Leucine
	2	2-Aminoethanol		21	2-Aminopimelic acid		40	Lysine
	3	docosanol		22	3-Aminoisobutyric acid		41	Methionine
	4	eicosanol		23	3-Aminopropanoic acid		42	Methionine sulfone
	5	ethylene glycol		24	3-Sulfinoalanine		43	N6-Acetyllysine
	6	Octopamine		25	4-Aminobutyric acid		44	N-Acetylaspartic acid
	7	Triethanolamine		26	4-Hydroxyproline		45	N-Acetylglutamine
amides	8	Allantoin		27	Alanine		46	Norvaline
	9	Creatinine		28	Arginine		47	Ornithine
	10	Glycyl-Glycine		29	Aspartic acid		48	Phenylalanine
	11	Oleamide		30	Cystathionine		49	Proline
	12	Pantothenic acid		31	Cysteine		50	Sarcosine
	13	Urea		32	Glutamic acid		51	Serine
amines	14	Cadaverine		33	Glutamic acid 5-methylester		52	Threonine
	15	Cystamine		34	Glutamine		53	Tryptophan
	16	Putrescine		35	Glycine		54	Tyrosine
	17	Spermidine		36	Histidine		55	Valine
amino acids	18	2-Aminoadipic acid		37	Isoleucine	carbo-hydrates	56	1,6-Anhydroglucose
	19	2-Aminobutyric acid		38	Kynurenine		57	2-Deoxy-glucose

Class	No	Metabolites	Class	No	Metabolites	Class	No	Metabolites
carbo-hydrates	58	6-Phosphogluconic acid	carbo-hydrates	77	Lyxose	carbo-hydrates	96	Threonic acid
	59	Allose		78	Maltose		97	Xylitol
	60	Arabinose		79	Mannitol		98	Xylose
	61	Dihydroxyacetone phosphate		80	Mannose		99	Xylulose
	62	Fructose		81	Mannose 6-phosphate	esters	100	gluconic acid lactone
	63	Galactitol		82	meso-Erythritol		101	O-Phosphoethanolamine
	64	Galactose		83	N-Acetylmannosamine	fatty acids	102	5-Aminovaleric acid
	65	Galacturonic acid		84	Psicose		103	Arachidonic acid
	66	Glucaric acid		85	Ribitol		104	Caproic acid
	67	Gluconic acid		86	Ribonolactone		105	Decanoic acid
	68	Glucono-1,5-lactone		87	Ribose		106	Docosahexaenoic acid
	69	Glucosamine		88	Ribose 5-phosphate		107	Eicosapentaenoic acid
	70	Glucose		89	Ribulose		108	Elaidic acid
	71	Glucose 6-phosphate		90	Ribulose 5-phosphate		109	heptadecanoic acid
	72	Glucuronic acid		91	Sedoheptulose 7-phosphate		110	lauric acid
	73	Glyceric acid		92	Sorbitol		111	Myristic acid
	74	Glycerol 3-phosphate		93	Sorbose		112	Nonanoic acid
	75	Inositol		94	Sucrose		113	Octanoic acid
	76	Lactitol		95	Tagatose		114	Oleic acid

Class	No	Metabolites	Class	No	Metabolites	Class	No	Metabolites
fatty acids	115	Palmitoleic acid	organic acids	133	3-Methyl-2-oxovaleric acid	organic acids	152	Phosphoenolpyruvic acid
	116	pentadecanoic acid		134	3-Phenyllactic acid		153	Pimelic acid
	117	Stearic acid		135	3-Phosphoglyceric acid		154	pyroglutamic acid
Indoles	118	5-Methoxytryptamine		136	4-Hydroxybenzoic acid		155	Pyruvic acid
	119	Tryptamine		137	5-Oxoproline		156	Salicylic acid
inorganic compounds	120	Hydroxylamine		138	Adipic acid		157	Sebacic acid
				139	Azelaic acid		158	Suberic acid
organic acids	121	2-Hydroxybutyric acid		140	Benzoic acid		159	Succinic acid
	122	2-Hydroxyglutaric acid		141	Citric acid		160	Taurine
	123	2-Hydroxyisobutyric acid		142	Fumaric acid	nucleosides	161	Cytidine
	124	2-Hydroxyisovaleric acid		143	Glutaric acid	phenols	162	Dopamine
	125	2-Ketoglutaric acid		144	Glycolic acid		163	Tyramine
	126	2-Ketoisocaproic acid		145	Hippuric acid	phosphoric acids	164	Phosphoric acid
	127	2-Phosphoglyceric acid		146	Hypotaurine			
	128	3-Aminoglutaric acid		147	Lactic acid	purines	165	7-Methylguanine
	129	3-Hydroxybutyric acid		148	Malic acid		166	Adenine
	130	3-Hydroxyisobutyric acid		149	Methylsuccinic acid		167	Adenosine
	131	3-Hydroxyisovaleric acid		150	Nicotinic acid		168	Guanine
	132	3-Hydroxypropionic acid		151	Oxalic acid		169	Guanosine

Class	No	Metabolites	Class	No	Metabolites	Class	No	Metabolites
purines	170	Hypoxanthine	pyridines	174	Niacinamide	steroids	178	Cholestanol
	171	Inosine	pyri-midines	175	Cytosine		179	Cholesterol
	172	Uric acid		176	Thymine	toco-pherols	180	alpha-tocopherol
	173	Xanthine		177	Uracil			

Alteration of metabolites induced by pentachlorophenol exposure

To analyze multivariate data for the clearer interpretation of the interclass variation, the PCA score plots and PLS-DA plot were used in the evalutaiotn of a metabolomics study (Trygg et al., 2007). In this study, two statistical models demonstrated that control and two treatment groups have significant differences in their metabolic profile. The PCA score plots for metabolites show that there are clear differences of metabolic profiles between the control and treatment groups (Figure 3). If the value of accumulated variance contribution rate (R^2X) is greater than 0.4, the difference among the three groups can be reliable result (Zhou et al., 2018). The R^2X value of the PCA result was 0.549, and it is reliable. PLS-DA also again, showed better clustering of individual three groups in a narrow area (Figure 4). The contribution rate of the supervision model (R^2Y) indicated PLS-DA model with differences among the groups are reliable and the model forecast rate (Q^2) values demonstrated the predictive ability of the model: in general, a robust mode has $Q^2 > 0.4$ (Li et al., 2015). In the PLS-DA plot, the R^2Y and Q^2 was calculated 0.936 and 0.8, respectively, demonstrating that control and two treatment groups have significant differences in their metabolic profile.

VIP analyses of PLS-DA model and p-value analyses of ANOVA model were conducted (Figure 5). The cutoff value for the VIP results was set at 1.0 with a standard error < 1.0, and the cutoff value for p-value of ANOVA was set 0.05 (Xia et al., 2010). Based on these criteria, 74 metabolites were identified as biomarkers that significantly contributed to distinguish metabolic profiles among three groups (Table 2). In metabolomic biomarkers, metabolites were mostly involved in amino acid (29%), carbohydrates (24%), or organic acid (20%). In figure 6, the 180 metabolites identified by GC-MS/MS and biomarkers selected by statistical values were distributed according to chemical class. Hierarchical clustering heatmap

unambiguously indicated the trends of metabolites changes (Figure 7). The color was constructed with the biomarker metabolites to intuitively identify the trends of metabolites changes in color from the highest (red) to lowest (blue). Hierarchical clustering analysis of the differential levels of metabolites related to those groups was performed on both samples (columns) and variables (rows), confirming clear separation with dendrogram among each three groups.

Figure 3. PCA plots of metabolites form zebrafish exposed to PCP. (Control group; 0 μg/L, Low group; 13 μg/L and High group; 130 μg/L).

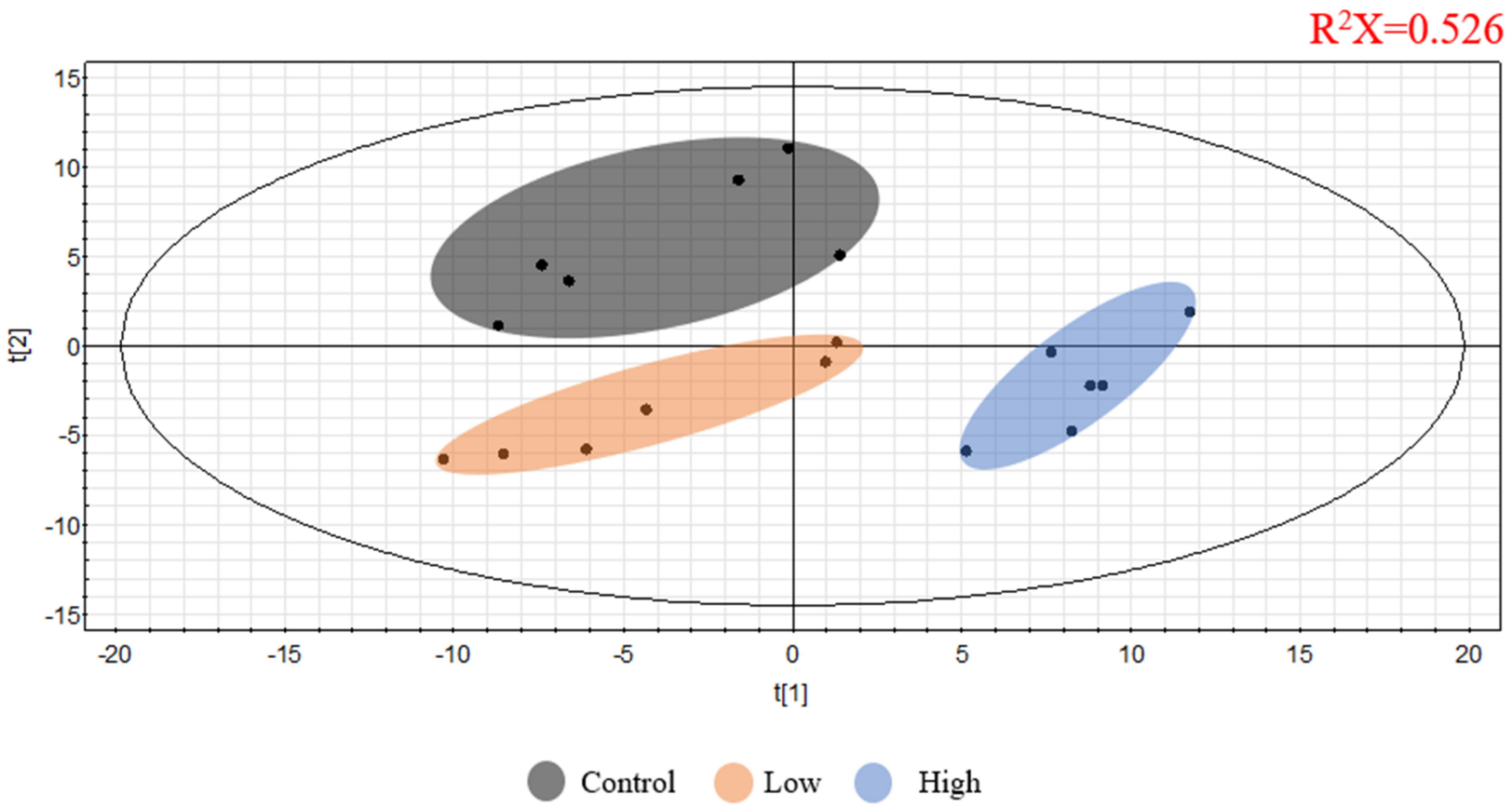
R²X=0.526
15
10
5
0
-5
-10
-15
t[2]
-20
-15
-10
-5
0
5
10
15
20
t[1]
Control
Low
High

Figure 4. PLS-DA plots of metabolites form zebrafish exposed to PCP. (Control group; 0 μg/L, Low group; 13 μg/L and High group; 130 μg/L).

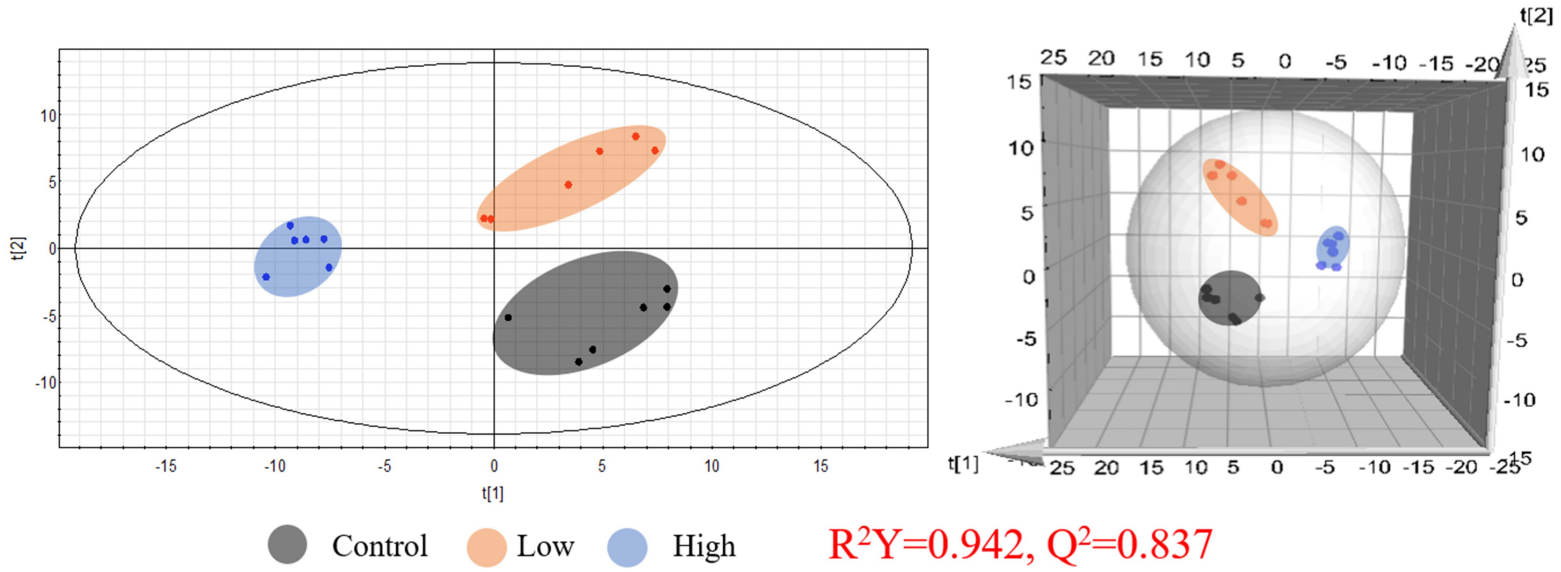
t[2]
t[1]
Control
Low
High
R²Y=0.942, Q²=0.837

Figure 5. Statistical analysis for metabolic biomarkers.

VIP value from PLSDA
(SIMCA-P+ 12.0.1)

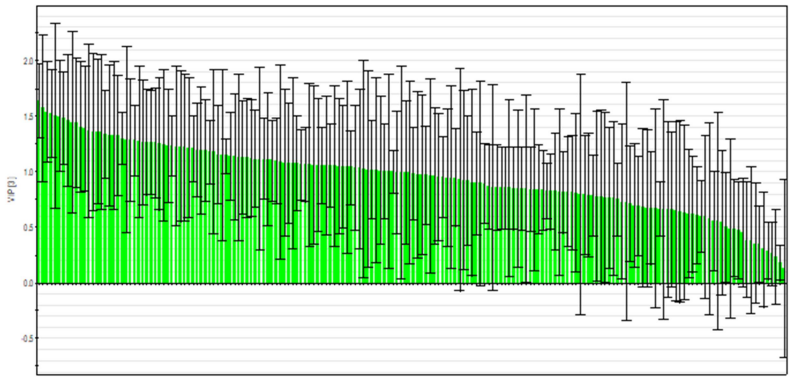

p-value from ANOVA
(Metaboanalyst 4.0)

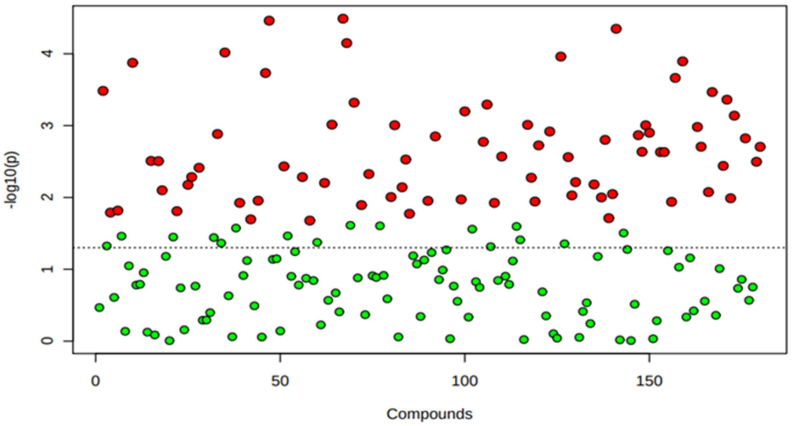

Table 2. Significantly altered metabolites in zebrafish exposed to pentachlorophenol (VIP > 1.0, SE < 1.0, p-value < 0.05).

No.	Compound name	VIP	Standard error	p.value
1	1-Hexadecanol	1.57	0.66	3.3.E-04
2	2-Aminoadipic acid	1.06	0.32	1.6.E-02
3	2-Aminobutyric acid	1.06	0.63	1.5.E-02
4	2-Aminoisobutyric acid	1.51	0.84	1.3.E-04
5	2-Hydroxyglutaric acid	1.25	0.60	3.1.E-03
6	2-Phosphoglyceric acid	1.20	0.42	3.1.E-03
7	3-Aminoisobutyric acid	1.05	0.72	7.9.E-03
8	3-Aminopropanoic acid	1.36	0.69	1.6.E-02
9	3-Hydroxypropionic acid	1.01	0.67	6.7.E-03
10	3-Phosphoglyceric acid	1.15	0.44	5.2.E-03
11	3-Sulfinoalanine	1.06	0.60	3.9.E-03
12	4-Hydroxybenzoic acid	1.08	0.66	1.3.E-03
13	6-Phosphogluconic acid	1.24	0.51	1.2.E-02
14	Adenine	1.27	0.68	2.0.E-02
15	Alanine	1.02	0.44	1.1.E-02
16	Allantoin	1.22	0.62	1.9.E-04
17	Arabinose	1.27	0.56	3.5.E-05
18	Arginine	1.33	0.67	3.7.E-03
19	Azelaic acid	1.32	0.54	5.2.E-03
20	Benzoic acid	1.40	0.59	6.3.E-03
21	Cholesterol	1.44	0.82	9.7.E-04
22	Cysteine	1.04	0.33	3.2.E-05
23	docosanol	1.37	0.78	7.1.E-05
24	eicosanol	1.50	0.50	4.8.E-04
25	ethylene glycol	1.54	0.45	4.7.E-03
26	Fructose	1.21	0.30	9.9.E-03
27	Galactitol	1.26	0.49	9.9.E-04
28	Gluconic acid	1.06	0.34	7.2.E-03
29	Glucuronic acid	1.02	0.84	3.0.E-03
30	Glutamic acid	1.23	0.72	1.1.E-02
31	Glutamine	1.08	0.77	1.4.E-03
32	Glutaric acid	1.15	0.77	6.3.E-04

No.	Compound name	VIP	Standard error	p.value
33	Guanine	1.12	0.82	1.7.E-03
34	heptadecanoic acid	1.48	0.42	5.1.E-04
35	Isoleucine	1.36	0.65	2.7.E-03
36	Lactic acid	1.06	0.73	9.8.E-04
37	Leucine	1.36	0.71	5.3.E-03
38	Lysine	1.26	0.47	1.1.E-02
39	Mannitol	1.46	0.60	1.9.E-03
40	Myristic acid	1.52	0.40	1.2.E-03
41	N6-Acetyllysine	1.01	0.43	1.1.E-04
42	N-Acetylaspartic acid	1.29	0.55	2.7.E-03
43	N-Acetylglutamine	1.19	0.57	9.4.E-03
44	Nicotinic acid	1.14	0.40	6.1.E-03
45	Octanoic acid	1.44	0.59	6.6.E-03
46	Oleamide	1.08	0.43	1.0.E-02
47	Oleic acid	1.33	0.64	1.6.E-03
48	O-Phosphoethanolamine	1.12	0.43	9.0.E-03
49	pentadecanoic acid	1.30	0.23	4.5.E-05
50	Phosphoenolpyruvic acid	1.10	0.36	1.4.E-03
51	Phosphoric acid	1.34	0.39	2.3.E-03
52	Proline	1.29	0.84	9.9.E-04
53	Psicose	1.23	0.27	1.3.E-03
54	pyroglutamic acid	1.05	0.55	2.3.E-03
55	Ribose	1.12	0.53	2.3.E-03
56	Ribose 5-phosphate	1.13	0.51	1.2.E-02
57	Ribulose	1.23	0.68	2.2.E-04
58	Ribulose 5-phosphate	1.13	0.56	1.3.E-04
59	Sebacic acid	1.13	0.53	1.0.E-03
60	Sedoheptulose 7-phosphate	1.05	0.37	2.0.E-03
61	Sorbitol	1.09	0.87	8.4.E-03
62	Sorbose	1.18	0.29	3.4.E-04
63	Stearic acid	1.64	0.33	3.6.E-03
64	Tagatose	1.11	0.37	4.4.E-04
65	Taurine	1.28	0.32	1.0.E-02
66	Threonine	1.22	0.66	7.3.E-04

No.	Compound name	VIP	Standard error	p.value
67	Thymine	1.24	0.69	1.5.E-03
68	Tryptophan	1.39	0.56	3.2.E-03
69	Tyramine	1.26	0.46	2.0.E-03
70	Tyrosine	1.10	0.39	2.7.E-02
71	Uracil	1.14	0.16	2.8.E-02
72	Valine	1.19	0.46	3.1.E-02
73	Xylose	1.06	0.34	3.6.E-02
74	Xylulose	1.17	0.74	4.7.E-02

Figure 6. Classification of metabolites. Distribution with total identified metabolites (left), and 74 metabolic biomarkers (right).

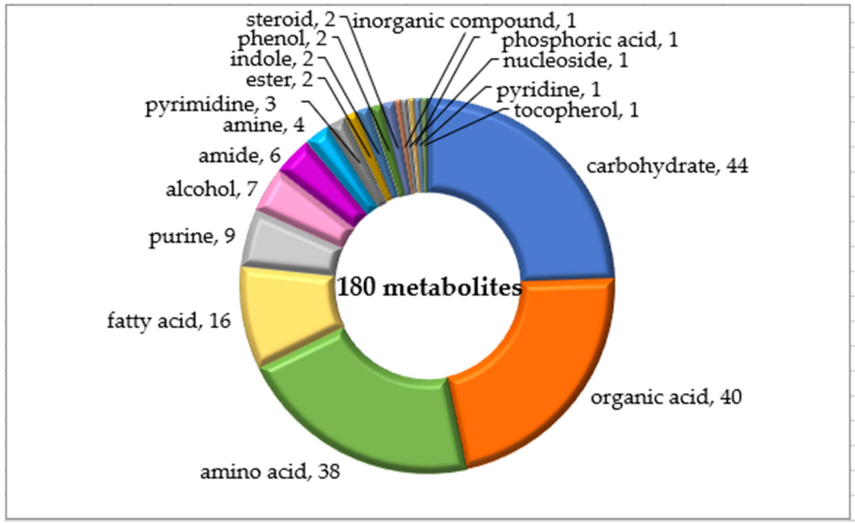
steroid, 2
inorganic compound, 1
phenol, 2
phosphoric acid, 1
indole, 2
nucleoside, 1
ester, 2
pyridine, 1
pyrimidine, 3
tocopherol, 1
amine, 4
amide, 6
carbohydrate, 44
alcohol, 7
purine, 9
180 metabolites
fatty acid, 16
organic acid, 40
amino acid, 38

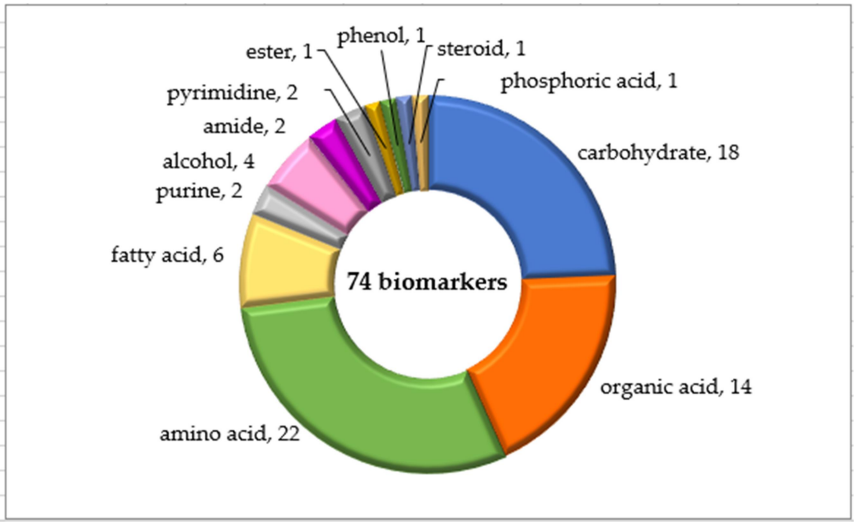
ester, 1
phenol, 1
steroid, 1
phosphoric acid, 1
pyrimidine, 2
amide, 2
carbohydrate, 18
alcohol, 4
purine, 2
fatty acid, 6
74 biomarkers
organic acid, 14
amino acid, 22

Figure 7. Hierarchical clustering heatmap analysis of 74 metabolite biomarkers in control (Con), low exposure (Low) and high exposure group (High).

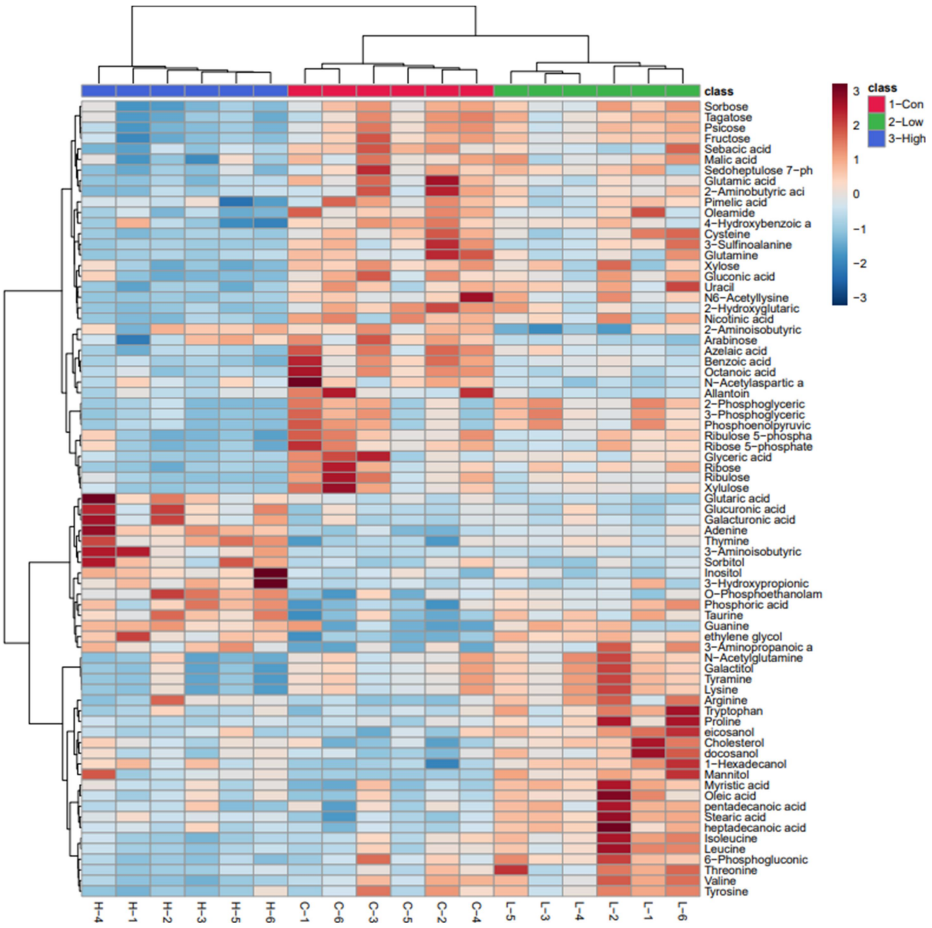
class
1−Con
2−Low
3−High
3
2
1
0
−1
−2
−3
Sorbose
Tagatose
Psicose
Fructose
Sebacic acid
Malic acid
Sedoheptulose 7−ph
Glutamic acid
2−Aminobutyric aci
Pimelic acid
Oleamide
4−Hydroxybenzoic a
Cysteine
3−Sulfinoalanine
Glutamine
Xylose
Gluconic acid
Uracil
N6−Acetyllysine
2−Hydroxyglutaric
Nicotinic acid
2−Aminoisobutyric
Arabinose
Azelaic acid
Benzoic acid
Octanoic acid
N−Acetylaspartic a
Allantoin
2−Phosphoglyceric
3−Phosphoglyceric
Phosphoenolpyruvic
Ribulose 5−phospha
Ribose 5−phosphate
Glyceric acid
Ribose
Ribulose
Xylulose
Glutaric acid
Glucuronic acid
Galacturonic acid
Adenine
Thymine
3−Aminoisobutyric
Sorbitol
Inositol
3−Hydroxypropionic
O−Phosphoethanolam
Phosphoric acid
Taurine
Guanine
ethylene glycol
3−Aminopropanoic a
N−Acetylglutamine
Galactitol
Tyramine
Lysine
Arginine
Tryptophan
Proline
eicosanol
Cholesterol
docosanol
1−Hexadecanol
Mannitol
Myristic acid
Oleic acid
pentadecanoic acid
Stearic acid
heptadecanoic acid
Isoleucine
Leucine
6−Phosphogluconic
Threonine
Valine
Tyrosine
H−4
H−1
H−2
H−3
H−5
H−6
C−1
C−6
C−3
C−5
C−2
C−4
L−5
L−3
L−4
L−2
L−1
L−6

Metabolic pathway and function analysis

Alteration of metabolites identified by metabolic profiling with GC-MS/MS makes it possible to predict changes in metabolism caused by toxic xenobiotics. MetaboAnalyst 4.0 (Chong et al., 2018), the comprehensive metabolomic data analysis system, has been widely used for identification of metabolic pathways based on metabolomic changes and high-quality KEGG (Kyoto Encyclopedia of Genes and Genomes) map. 74 Biomarker metabolites were investigated with the pathway analysis module of MetaboAnalyst 4.0, and it shows several significant metabolic pathways considering variation pattern with metabolites based on 3 groups (control and two groups exposed to pentachlorophenol). Biomarker metabolites contributing to the complete separation of pentachlorophenol exposed to zebrafish from healthy controls identified eight key metabolic pathways such pentose phosphate pathway, pentose and glucuronate interconversions, taurine and hypotaurine metabolism, glutamine and glutamate metabolism, alanine, aspartate and glutamate metabolism, β-alanine metabolism, ascorbate and aldarate metabolism and phenylalanine metabolism (Figure 8). Alteration of some metabolites may estimate the changes of metabolism in the zebrafish when exposed to PCP (Figure 9).

Decrease in metabolites could mean that they were used for synthesis of new metabolites, or it could mean that defects of metabolites due to damage such as inhibition of enzymes would have an adverse effect in living organisms (Guo et al., 2014; Lee et al., 2020). There was a decrease of biomarkers in several pathways in this study. Most of metabolites in pentose phosphate pathway (PPP) decreased depending on the concentration of PCP, and it may be expected to induce PCP-induced damage in zebrafish. Indeed, PCP exposure in human erythrocytes inhibit the activities of enzymes of both glycolysis and pentose phosphate shunt (Maheshwari et al., 2019). The main role of PPP is the synthesis

of ribonucleotide, the basic building blocks of RNA, and NADPH which is a molecular precursor of fatty acid synthesis and blocking source of reactive oxygen species (ROS) (Stincone et al., 2015). If the activity of PPP would be attenuated by PCP, it makes zebrafish more vulnerable to oxidants due to reduction of a scavenger of ROS (Carson et al., 1956; Ralser et al., 2007). Oxidative stress might contribute to carcinogenesis by induction of genetic modifications (Khansari et al., 2009), so PCP could cause fatal injuries to the zebrafish.

There was also increase of biomarkers in several pathways in this study. The level of glucuronic acid, 3-hydroxypropionate and taurine increased in exposure groups compared with that in control group. Glucuronic acid is tightly correlated with synthesis of ascorbate. The two pathways (ascorbate and aldarate metabolism, pentose and glucuronate interconversions) are known for relation with better survival for cancer patients (Xie et al., 2019). Ascorbate is a powerful reducing agent capable of rapidly scavenging ROS, and it is used to regulate lipid peroxidation (Brunet et al., 2000). Increasing amount of glucuronic acid indicates that the body was stimulated to release more ascorbate to inhibit inflammatory reaction (Bernotti et al., 2003). Moreover, 3-hydroxy propionate (3-HP) is related to propionate metabolism according to KEGG map. The propionate is able to counteract cancer cell proliferation in the liver tissue and also induce cell apoptosis in lung cancer (Bindels et al., 2012; Kim et al., 2019). So if the increase of 3-HP is related to the activation of propionate metabolism, it may protect the zebrafish against PCP. Taurine and hypotaurine metabolism also improved in this similar way. Taurine is also known as a useful antioxidant to hinder the increase of ROS in tumors, leading to delay of the development of cancer. (El Agouza et al., 2011). Considering only the perturbation of metabolites, we would presume increase of these metabolites protects cells from oxidative stress leading to cytotoxicity as an effective antioxidant and treat the cancer in the zebrafish exposed to PCP. However, in order to more accurately understand the disruption

of metabolic processes that occur by PCP exposure, it is not enough to interpret with the level of metabolites alone. To reduce the possibility of misunderstanding about interpretation, it is necessary to be linked with proteomics.

Figure 8. Metabolic pathway plot generated from metabolome biomarkers

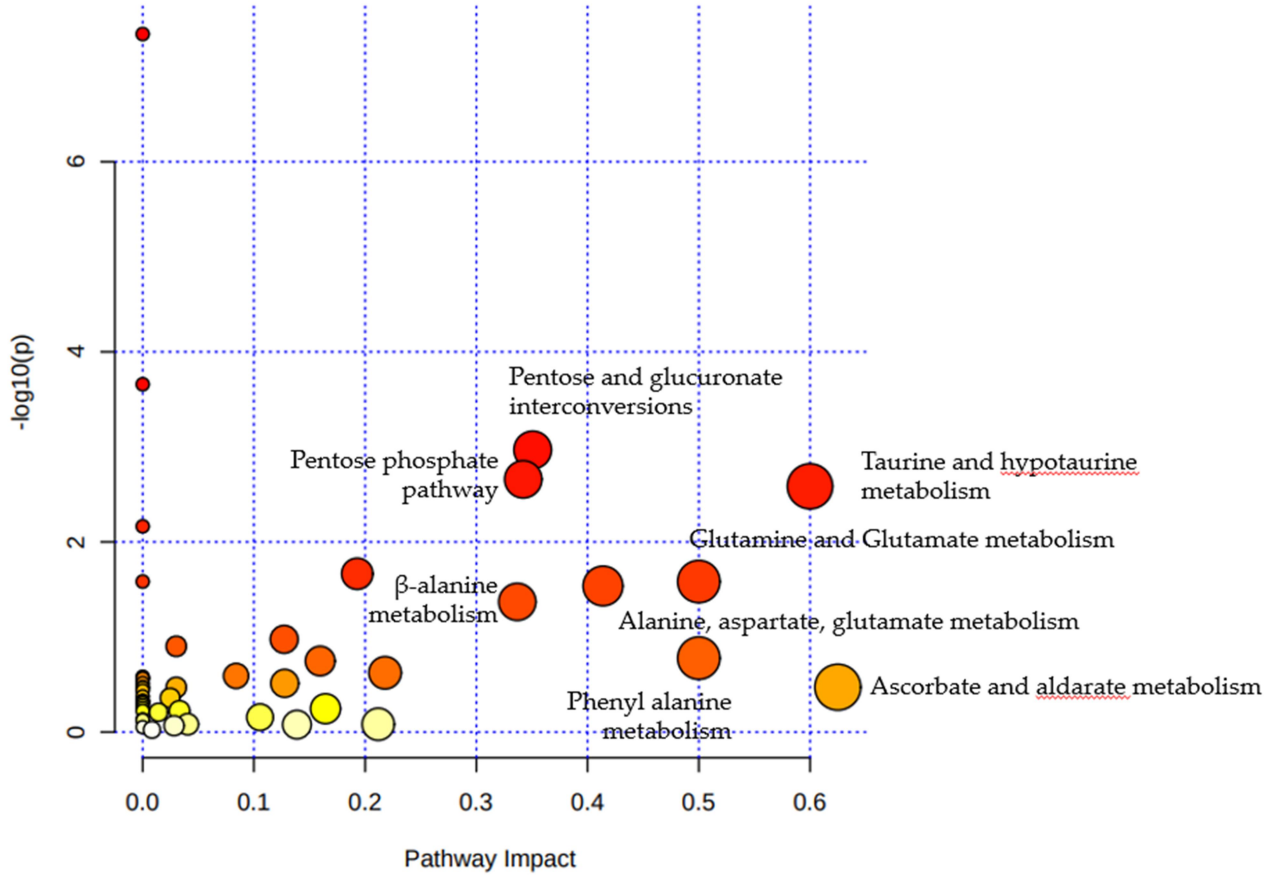
-log10(p)
0
2
4
6
0.0
0.1
0.2
0.3
0.4
0.5
0.6
Pathway Impact
Pentose and glucuronate interconversions
Pentose phosphate pathway
Taurine and hypotaurine metabolism
Glutamine and Glutamate metabolism
β-alanine metabolism
Alanine, aspartate, glutamate metabolism
Ascorbate and aldarate metabolism
Phenyl alanine metabolism

Figure 9. Perturbed pathways and fluctuating metabolites in zebrafish whole body induced by pentachlorophenol exposure. The graphs represent the average relative areas of each metabolite and significantly different changes of $p < 0.05$ and $p < 0.005$ in relative areas are labeled by "*" and "**", respectively. The color of box represents group of each metabolomes: Red (increased metabolite biomarker), Blue (decreased metabolite biomarker), and Gray (predicted metabolite related to pathway).

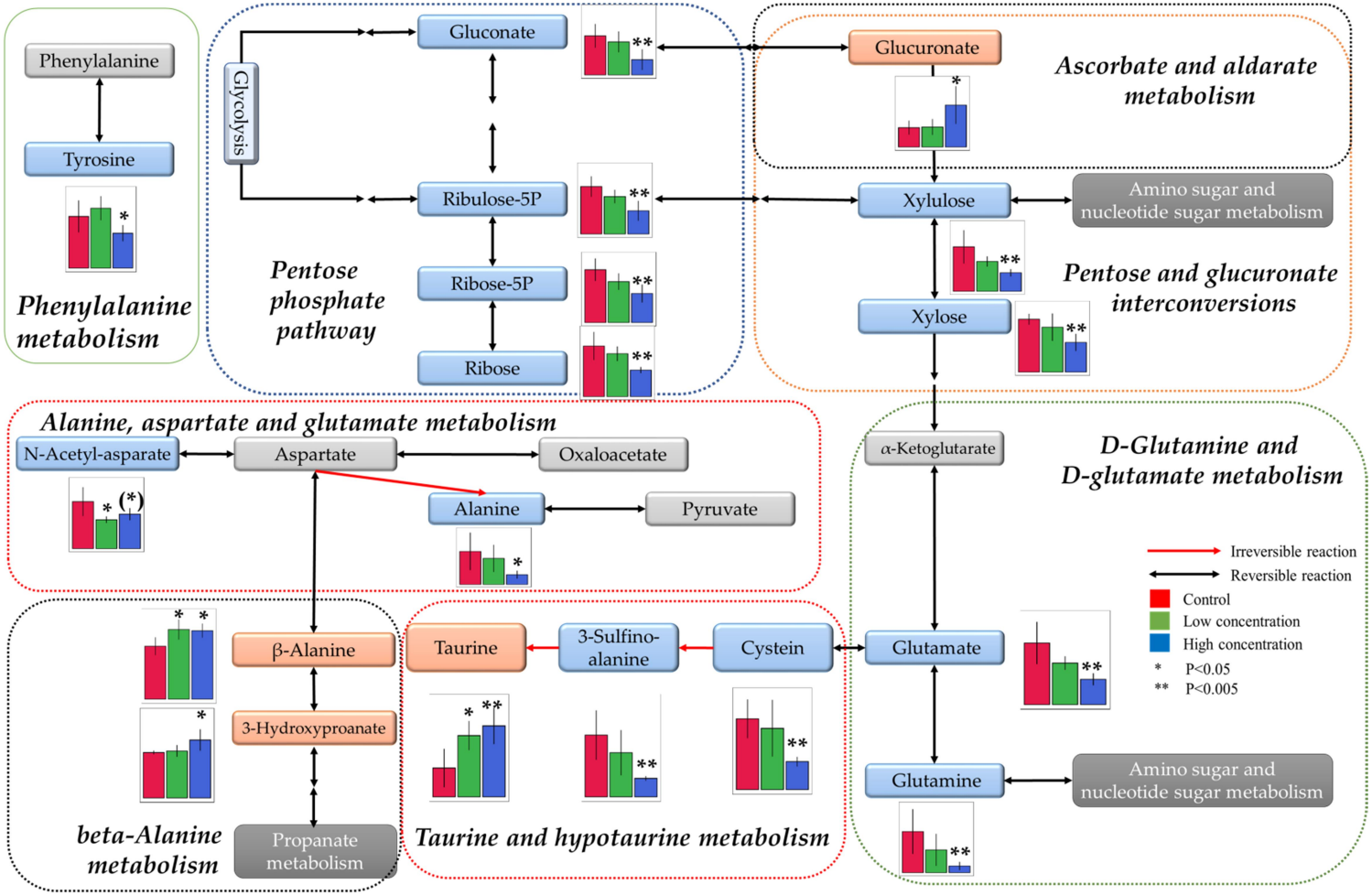
Phenylalanine
Tyrosine
Phenylalanine metabolism
Glycolysis
Gluconate
Ribulose-5P
Ribose-5P
Ribose
Pentose phosphate pathway
Glucuronate
Ascorbate and aldarate metabolism
Xylulose
Amino sugar and nucleotide sugar metabolism
Xylose
Pentose and glucuronate interconversions
Alanine, aspartate and glutamate metabolism
N-Acetyl-asparate
Aspartate
Oxaloacetate
Alanine
Pyruvate
β-Alanine
3-Hydroxyproanate
Propanate metabolism
beta-Alanine metabolism
Taurine
3-Sulfino-alanine
Cystein
Taurine and hypotaurine metabolism
α-Ketoglutarate
Glutamate
Glutamine
Amino sugar and nucleotide sugar metabolism
D-Glutamine and D-glutamate metabolism
Irreversible reaction
Reversible reaction
Control
Low concentration
High concentration
* P<0.05
** P<0.005

Oxidative stress induced by PCP

To confirm oxidative stress caused by PCP exposure, ROS and MDA assay test (n=3) were conducted. The amount of ROS was detected by DCFH-DA assays. MDA, one of the major products of lipid peroxidation in cell membranes, is used as an index of lipid oxidation (Mateos et al., 2005). The calibration curves for each assay were showed with r^2 >0.99, indicating great linearity (Figure 10). Even though ROS production did not show statistically significant difference, the increase of ROS was clearly observed while MDA of exposure groups significantly increased ($p < 0.05$), suggesting oxidative damage of cell (Figure 11).

Figure 10. Calibration curve for protein, ROS, and MDA

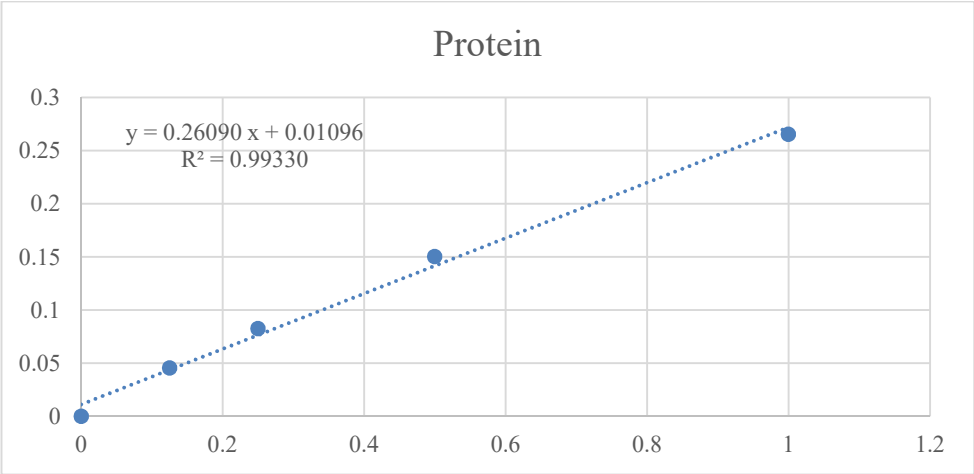
Protein
y = 0.26090 x + 0.01096
R² = 0.99330
0.3
0.25
0.2
0.15
0.1
0.05
0
0
0.2
0.4
0.6
0.8
1
1.2

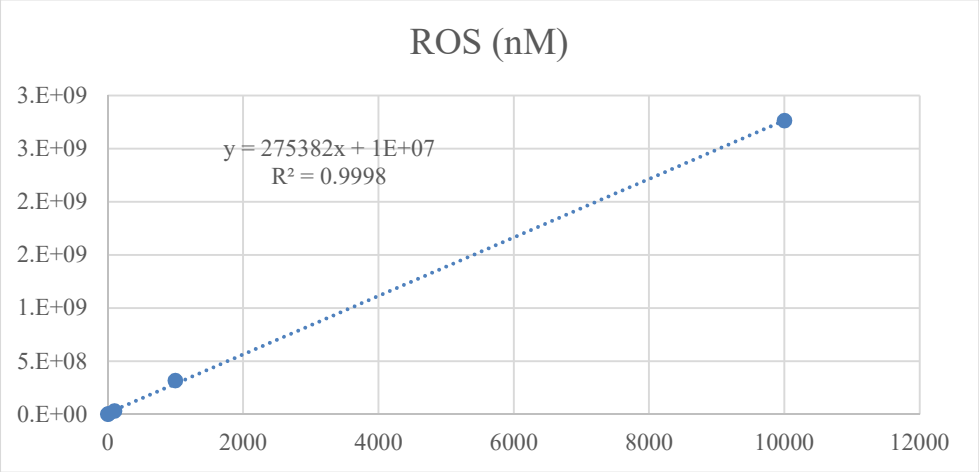
ROS (nM)
y = 275382x + 1E+07
R² = 0.9998
3.E+09
3.E+09
2.E+09
2.E+09
1.E+09
5.E+08
0.E+00
0
2000
4000
6000
8000
10000
12000

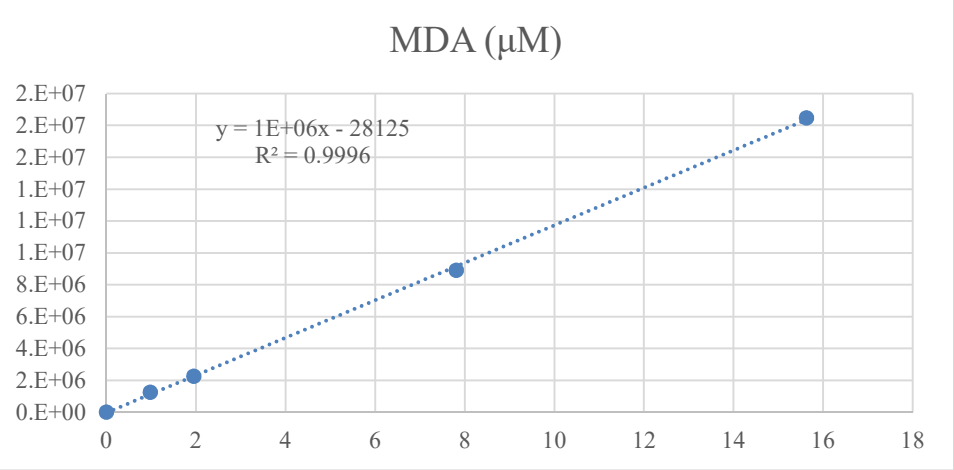
MDA (µM)
y = 1E+06x - 28125
R² = 0.9996
2.E+07
2.E+07
2.E+07
1.E+07
1.E+07
1.E+07
8.E+06
6.E+06
4.E+06
2.E+06
0.E+00
0
2
4
6
8
10
12
14
16
18

Figure 11. Levels of ROS (A) and MDA (B) in three groups (*$p < 0.05$).

(A)

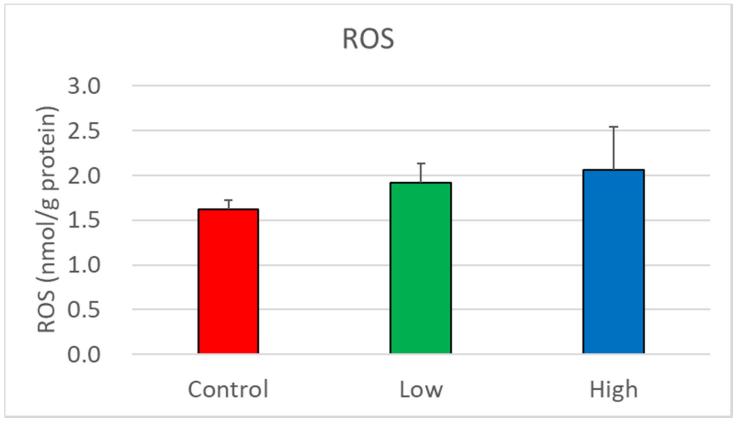
ROS
ROS (nmol/g protein)
3.0
2.5
2.0
1.5
1.0
0.5
0.0
Control
Low
High

(B)

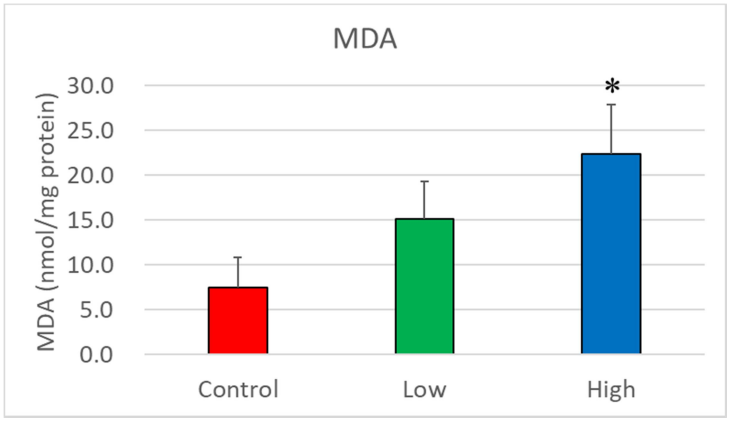
MDA
MDA (nmol/mg protein)
30.0
25.0
20.0
15.0
10.0
5.0
0.0
*
Control
Low
High

Proteome profiling, proteome biomarker and gene ontology

Each macerated sample of zebrafish from control and high exposure for 48h was pooled for proteomic profiling and protein content was quantitated before comprehensive sample preparation using filter-aided sample preparation (FASP) method (Diz et al., 2009; Wiśniewski et al., 2009). Protein was quantitated for proteomic analysis and 2108 proteins were identified after processing of analytical data with Proteome Discoverer (Figure 12). Those proteins were evaluated by volcano plot with p-value (< 0.05) and fold change (< 0.5 or > 2.0) to result in 376 protein biomarkers that significantly contributed to distinguish proteomic profiles between two groups (Figure 13) (Table 3) (Matés et al., 2012; Gupta et al., 2018). Each number of down regulation (fold change <0.5) and up regulation (fold change > 2.0) was 91 and 285, respectively. Eleven proteins were identified only in exposure group among 376 proteomic biomarkers, 41 proteins only in the control group, and 324 proteins were observed commonly in the both groups (Figure 14). To get more insight into the subcellular origin of the identified proteins, gene ontology (GO) for the functional enrichment analysis was done with WebGestalt (web-based gene set analysis toolkit), classifying genes into biologically functional groups (Gene, 2015). From gene ontology (GO) analysis, proteins mostly involved in biological process, cellular component and molecular function were classified. In biological process, proteins were mostly located in metabolic process (107), biological regulation (59), or cellular component organization (59). Mainly protein-containing complex (54), nucleus (37), or membrane (35) was involved in cellular component. As for molecular function, most proteomic biomarkers were observed in ion binding (56), protein binding (44), or hydrolase activity (38) (Figure 15).

Figure 12. TIC of proteins in zebrafish samples in control group (A) and pentachlorophenol (130 μg/L) exposed group (B).

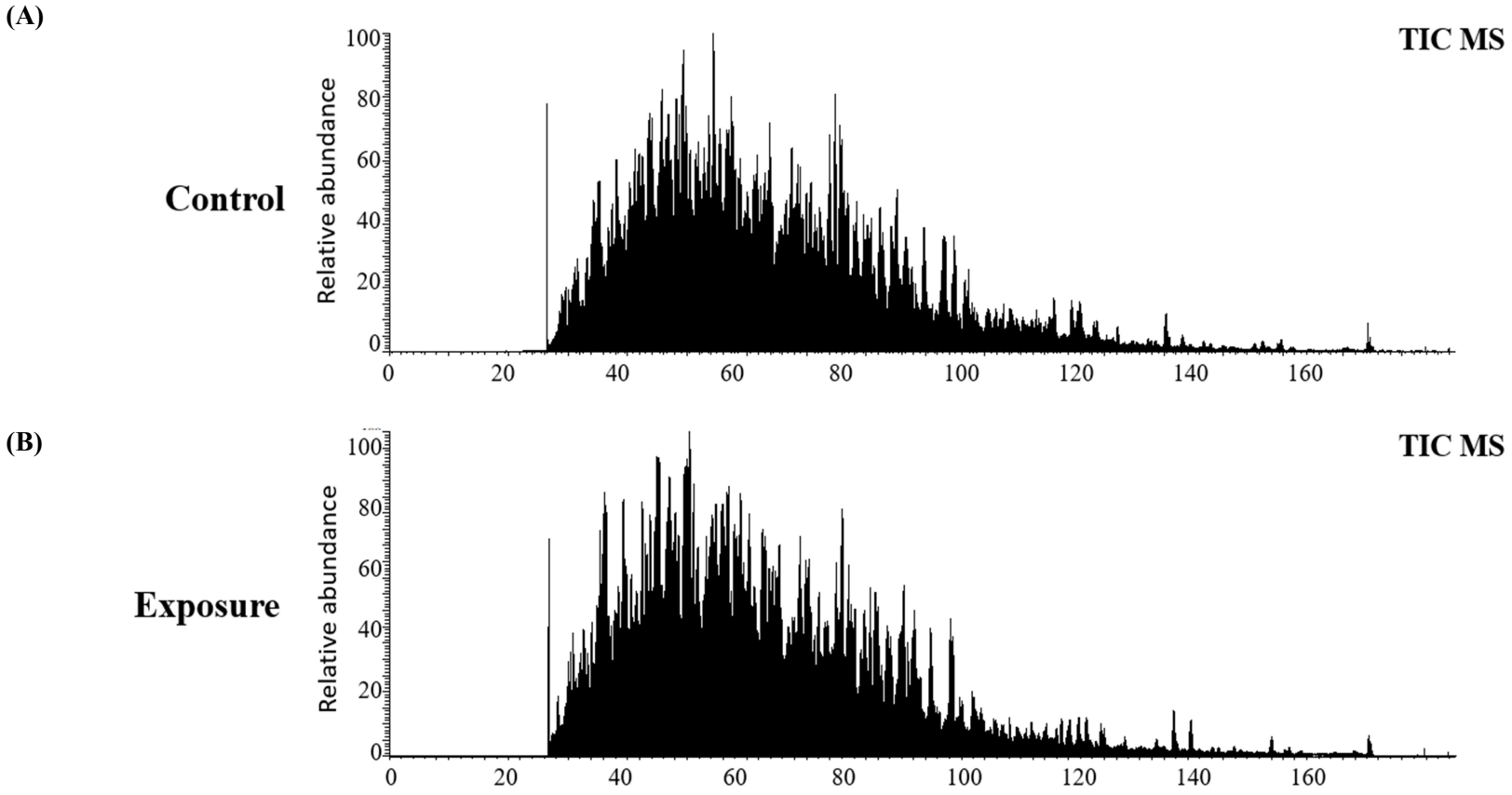
(A)
Control
TIC MS
Relative abundance
100
80
60
40
20
0
0
20
40
60
80
100
120
140
160
(B)
Exposure
TIC MS
Relative abundance
100
80
60
40
20
0
0
20
40
60
80
100
120
140
160

Figure 13. Volcano plots of total identified proteins. Pink dots indicate biomarker proteins with differences between groups selected according to the threshold (p-value < 0.05 and fold change > 2.0).

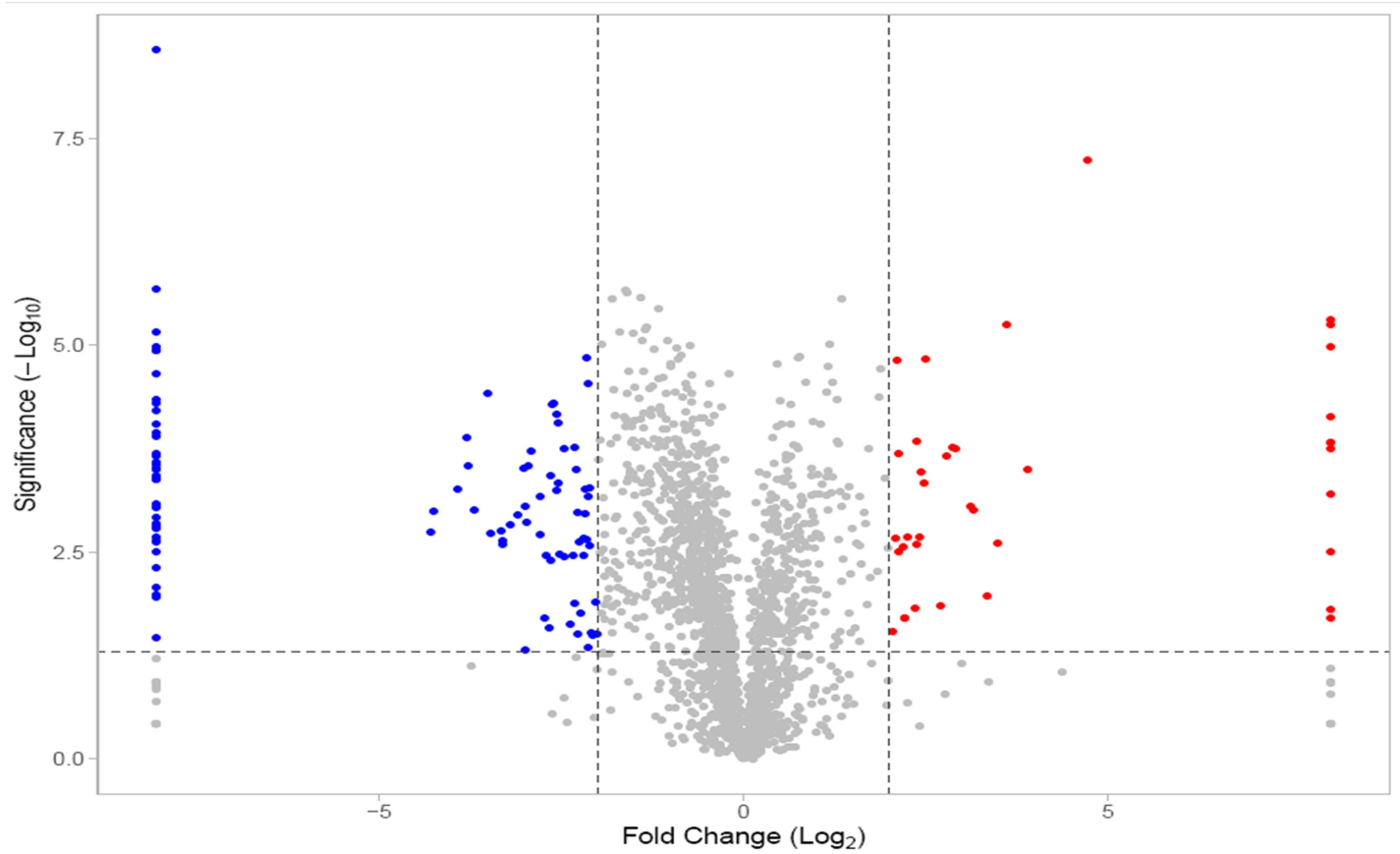
7.5
5.0
2.5
0.0
Significance (−Log10)
−5
0
5
Fold Change (Log2)

Table 3. Significantly altered biomarker proteins in zebrafish exposed to pentachlorophenol which were selected from proteomics approach.

No.	Accesion	Description	Gene Symbol	p-value	Fold change	$\log_2$ (FC)
1	NP_001304118.1	unconventional myosin-Ic	myo1cb	2.69E-09	0.00	-8.06
2	AAI15301.1	Zgc:136871	mat2al	2.09E-06	0.00	-8.06
3	NP_997050.1	parvalbumin isoform 2a	pvalb5	6.88E-06	0.00	-8.06
4	AAI54333.1	Xrcc6 protein	xrcc6	1.06E-05	0.00	-8.06
5	AAI55199.1	Pepd protein	pepd	1.17E-05	0.00	-8.06
6	AAT68084.1	v-ATPase AC39 subunit	atp6v0d1	1.17E-05	0.00	-8.06
7	AAP59458.1	transketolase	tktb	2.23E-05	0.00	-8.06
8	NP_001070932.2	myosin heavy chain 7-like	vmhcl	4.57E-05	0.00	-8.06
9	XP_021331997.1	ubiquitin-associated domain-containing protein 1 isoform X1	ubac1	5.11E-05	0.00	-8.06
10	XP_017207982.1	elongation factor 1-delta isoform X1	eef1db	6.24E-05	0.00	-8.06
11	Q6DGY7.1	RecName: Full=Gamma-crystallin N-B; AltName: Full=Gamma-N-crystallin-B; AltName: Full=Gamma-N2-crystallin	crygn2	9.03E-05	0.00	-8.06
12	XP_021326446.1	mucin-2	muc2.1	1.15E-04	0.00	-8.06
13	NP_001104010.1	cytochrome c oxidase assembly protein COX19	cox19	1.25E-04	0.00	-8.06
14	AAH76262.1	VAMP (vesicle-associated membrane protein)-associated protein A, like	vapal	2.04E-04	0.00	-8.06
15	AAH80251.1	Cystathionase (cystathionine gamma-lyase), like	cthl	2.20E-04	0.00	-8.06
16	XP_005157918.1	sorcin isoform X1	sri	2.60E-04	0.00	-8.06

No.	Accesion	Description	Gene Symbol	p-value	Fold change	log_2 (FC)
17	NP_001017593.1	epithelial cell adhesion molecule	epcam	2.81E-04	0.00	-8.06
18	NP_001003528.1	tissue specific transplantation antigen P35B	zgc:100864	3.07E-04	0.00	-8.06
19	Q6AZW2.2	RecName: Full=Aldo-keto reductase family 1 member A1-A; AltName: Full=Alcohol dehydrogenase [NADP(+)] A; AltName: Full=Aldehyde reductase-A	akr1a1a	3.22E-04	0.00	-8.06
20	XP_005166169.1	calcium-dependent secretion activator 1 isoform X1	cadpsb	3.77E-04	0.00	-8.06
21	XP_009290735.1	uncharacterized protein LOC678541 isoform X1	gstk4	4.06E-04	0.00	-8.06
22	NP_998215.1	chitinase, acidic.1 precursor	chia.1	4.22E-04	0.00	-8.06
23	XP_009292643.1	protein argonaute-2 isoform X1	ago2	4.22E-04	0.00	-8.06
24	AAC60097.1	enhancer of rudimentary homolog	erh	8.37E-04	0.00	-8.06
25	NP_956090.1	bridging integrator 2	bin2b	8.89E-04	0.00	-8.06
26	XP_698092.2	gamma-crystallin M2	crygm2e	9.05E-04	0.00	-8.06
27	XP_009296495.1	excitatory amino acid transporter 2 isoform X2	slc1a2b	9.19E-04	0.00	-8.06
28	NP_956324.1	60S ribosomal protein L27a	rpl27a	1.23E-03	0.00	-8.06
29	XP_009302755.1	myc box-dependent-interacting protein 1-like isoform X2	LOC563561	1.41E-03	0.00	-8.06
30	AAI29260.1	Zgc:136272	si:rp71-1g18.7	1.47E-03	0.00	-8.06
31	AAQ91233.1	dihydrolipoamide dehydrogenase	dldh	1.52E-03	0.00	-8.06
32	NP_001002456.1	histone-lysine N-methyltransferase SETD7	setd7	1.59E-03	0.00	-8.06
33	XP_021326447.1	mucin-2-like, partial	LOC110438407	2.11E-03	0.00	-8.06

No.	Accesion	Description	Gene Symbol	p-value	Fold change	log_2 (FC)
34	AAI53586.1	Zgc:92501	galm	2.36E-03	0.00	-8.06
35	XP_002667589.3	intestinal mucin-like protein isoform X2	LOC100332723	2.36E-03	0.00	-8.06
36	AAI64248.1	Bccip protein	bccip	3.15E-03	0.00	-8.06
37	NP_998703.1	crk-like protein	crkl	4.98E-03	0.00	-8.06
38	NP_991124.2	double-stranded RNA-binding protein Staufen homolog 1	stau1	8.39E-03	0.00	-8.06
39	Q7SXS7.1	RecName: Full=Actin-histidine N-methyltransferase; AltName: Full=SET domain-containing protein 3	setd3	1.04E-02	0.00	-8.06
40	XP_009300420.1	myosin-10 isoform X1	myh10	1.10E-02	0.00	-8.06
41	AAI64282.1	Rps16 protein	rps16	3.43E-02	0.00	-8.06
42	NP_001002683.1	dipeptidyl peptidase 3	dpp3	1.81E-03	0.05	-4.28
43	AAH85386.1	Nucleosome assembly protein 1-like 4b	nap1l4b	1.04E-03	0.05	-4.26
44	XP_005174376.3	anamorsin isoform X1	ciapin1	5.50E-04	0.07	-3.93
45	AAQ97774.1	eukaryotic translation initiation factor 3, subunit 7 zeta, 66/67kDa	eif3d	1.33E-04	0.07	-3.79
46	AAI65383.1	Ppp2ca protein	ppp2ca	2.88E-04	0.07	-3.78
47	AAH59677.1	Zgc:73367	rps28	9.90E-04	0.08	-3.68
48	AAH63968.1	Rho GDP dissociation inhibitor (GDI) alpha	arhgdia	3.85E-05	0.09	-3.50
49	XP_005159433.1	tropomyosin alpha-3 chain isoform X2	tpm3	1.87E-03	0.09	-3.48
50	AAH65609.1	Chloride intracellular channel 4	clic4	1.79E-03	0.10	-3.33
51	AAI71497.1	Lpp protein	lpp	2.30E-03	0.10	-3.31

No.	Accesion	Description	Gene Symbol	p-value	Fold change	log_2 (FC)
52	AAI15161.1	Dnl2 protein, partial	dynll2a	1.48E-03	0.11	-3.20
53	XP_021324071.1	3'(2'),5'-bisphosphate nucleotidase 1 isoform X1	bpnt1	1.12E-03	0.12	-3.09
54	AAH76251.1	S100 calcium binding protein, beta (neural)	s100b	3.07E-04	0.12	-3.01
55	AAH53413.1	Heterogeneous nuclear ribonucleoprotein R	hnrnpr	8.95E-04	0.13	-2.99
56	AAQ13341.1	guanidinoacetate N-methyltransferase	gamt	4.90E-02	0.13	-2.99
57	AAH49337.1	Translocase of outer mitochondrial membrane 34	tomm34	1.40E-03	0.13	-2.98
58	NP_956352.1	receptor expression-enhancing protein 5	reep5	2.93E-04	0.13	-2.95
59	NP_958915.1	mitogen-activated protein kinase 3	mapk3	1.91E-04	0.13	-2.92
60	AAI71423.1	Calpain 2, (m/II) large subunit b	capn2b	1.93E-03	0.14	-2.80
61	F1QEG2.1	RecName: Full=Kelch-like protein 41b; AltName: Full=Kelch repeat and BTB domain-containing protein 10b	klhl41b	6.81E-04	0.14	-2.79
62	AAS92647.1	karyopherin alpha 4	kpna4	2.01E-02	0.15	-2.73
63	AAI64384.1	Cab39 protein	cab39l1	3.53E-03	0.15	-2.71
64	NP_001006046.1	copper homeostasis protein cutC homolog	cutc	2.66E-02	0.16	-2.67
65	AAQ62127.1	short chain dehydrogenase/reductase	flj13639	3.83E-04	0.16	-2.65
66	ALA04606.1	recoverin-1a	rcvrna	3.98E-03	0.16	-2.65
67	AAH71392.1	Zgc:86715	ppil3	5.24E-05	0.16	-2.62
68	AAH95279.1	Iah1 protein, partial	iah1	5.08E-05	0.16	-2.61
69	NP_001028922.1	alanine--glyoxylate aminotransferase 2, mitochondrial	agxt2	5.73E-04	0.17	-2.57

No.	Accesion	Description	Gene Symbol	p-value	Fold change	log_2 (FC)
70	AAH45328.1	Protein tyrosine phosphatase, non-receptor type 11 (Noonan syndrome 1)	ptpn11a	6.92E-05	0.17	-2.56
71	NP_001003984.1	signal transducer and activator of transcription 5b	stat5b	8.74E-05	0.17	-2.55
72	NP_001004573.2	O-acetyl-ADP-ribose deacetylase MACROD1	macrod1	4.73E-04	0.17	-2.54
73	NP_001002079.1	40S ribosomal protein S13	rps13	3.35E-03	0.17	-2.53
74	NP_001038898.2	ribosomal protein S5-like	zgc:153322	1.79E-04	0.18	-2.47
75	AAQ18217.1	Ran-binding protein 7, partial	ipo7	3.62E-03	0.18	-2.46
76	NP_001074047.2	cytosolic endo-beta-N-acetylglucosaminidase	engase	2.36E-02	0.19	-2.37
77	Q4VBV9.1	RecName: Full=Omega-amidase NIT2; AltName: Full=Nitrilase homolog 2	nit2	3.45E-03	0.20	-2.34
78	NP_001004527.2	serine/threonine-protein phosphatase PP1-beta catalytic subunit	ppp1cb	1.31E-02	0.20	-2.32
79	NP_956878.1	glutathione S-transferase theta 1b	gstt1b	1.74E-04	0.20	-2.32
80	AAI71716.1	Translocase of outer mitochondrial membrane 70 homolog A (yeast)	tomm70a	3.23E-04	0.20	-2.29
81	NP_001296417.1	UPF0160 protein MYG1, mitochondrial	myg1	1.05E-03	0.21	-2.28
82	XP_005161033.1	phytanoyl-CoA dioxygenase domain-containing protein 1 isoform X2	phyhd1	3.10E-02	0.21	-2.27
83	NP_001013519.1	calpain 2, (m/II) large subunit a	capn2a	2.39E-03	0.21	-2.25
84	AAH56521.1	Splicing factor 3a, subunit 1	sf3a1	1.75E-02	0.21	-2.24
85	NP_001002117.1	ribokinase	rbks	3.44E-03	0.22	-2.20
86	Q9PV90.1	RecName: Full=60S acidic ribosomal protein P0; AltName: Full=60S ribosomal protein L10E	rplp0	2.14E-03	0.22	-2.18
87	NP_001017899.2	calpain small subunit 1	capns1a	5.43E-04	0.22	-2.16

No.	Accesion	Description	Gene Symbol	p-value	Fold change	log_2 (FC)
88	AAI54795.1	UDP-glucose dehydrogenase	ugdh	2.21E-03	0.22	-2.16
89	XP_005158038.1	uncharacterized protein LOC436616	zgc:92184	1.43E-05	0.22	-2.15
90	NP_001138274.1	si:ch211-251b21.1 precursor	si:ch211-251b21.1	4.49E-02	0.23	-2.14
91	AAI64891.1	Zgc:92880 protein	hbba2	2.90E-05	0.23	-2.13
92	NP_001035411.2	cold-inducible RNA-binding protein isoform 1	cirbpb	6.70E-04	0.23	-2.13
93	XP_005159798.1	proteasome subunit beta type-4 isoform X1	psmb4	5.25E-04	0.23	-2.12
94	AAH92740.1	Carbonic anhydrase VIII	ca8	2.69E-03	0.23	-2.11
95	NP_999877.1	AH receptor-interacting protein	aip	2.96E-02	0.24	-2.09
96	AAF98361.1	Na+/K+ ATPase beta subunit isoform 1	atp1b1a	3.23E-02	0.24	-2.06
97	AAI52672.1	Zgc:64031	abhd14b	1.29E-02	0.25	-2.03
98	AAH76321.1	Ribosomal protein L35a	rpl35a	3.14E-02	0.25	-2.02
99	AAH76196.1	Zgc:92716	psma6b	2.44E-04	0.25	-1.99
100	AAI53575.1	Glyoxalase domain containing 4	glod4	1.39E-04	0.25	-1.98
101	AAQ97819.1	NDRG family member 3	ndrg3a	3.27E-03	0.26	-1.97
102	AAH56700.1	Proteasome activator subunit 2	psme2	9.69E-06	0.26	-1.95
103	XP_017213163.1	tropomyosin alpha-4 chain isoform X1	tpm4b	1.76E-02	0.26	-1.95
104	Q5U3U3.2	RecName: Full=Carnitine O-palmitoyltransferase 2, mitochondrial; AltName: Full=Carnitine palmitoyltransferase II; Short=CPT II; Flags: Precursor	cpt2	2.96E-03	0.26	-1.93

No.	Accesion	Description	Gene Symbol	p-value	Fold change	log_2 (FC)
105	AAI71364.1	Ckmt2 protein	ckmt2b	7.11E-04	0.26	-1.92
106	AAQ97767.1	DNA-damage inducible protein 2	ddi2	2.07E-02	0.27	-1.91
107	AAI64767.1	Zgc:153353 protein	agmat	6.20E-03	0.27	-1.91
108	XP_005162977.1	slow myosin heavy chain 1 isoform X1	smyhc1	1.92E-03	0.27	-1.91
109	AAI15074.1	LOC100004902 protein, partial	erp27	1.20E-03	0.27	-1.90
110	CAK04652.1	novel protein similar to tyrosine aminotransferase (TAT), partial	tat	1.39E-02	0.27	-1.90
111	NP_001002343.1	guanylate binding protein 1	gbp1	3.99E-03	0.27	-1.90
112	XP_005163928.1	40S ribosomal protein S2 isoform X1	rps2	1.17E-02	0.27	-1.87
113	AAH65884.1	Rp42 homolog (pending)	dcun1d2a	5.27E-03	0.28	-1.84
114	NP_001003559.1	fucosidase, alpha-L-1, tissue precursor	fuca1.2	8.71E-03	0.28	-1.84
115	XP_002667598.5	prolyl endopeptidase-like, partial	LOC100334014	1.55E-04	0.28	-1.82
116	AAH67628.1	Twinfilin, actin-binding protein, homolog 1a	twf1a	1.45E-02	0.29	-1.81
117	XP_005172875.1	thimet oligopeptidase isoform X1	thop1	1.42E-02	0.29	-1.81
118	NP_001071253.1	vacuolar protein sorting-associated protein 37C	vps37c	2.97E-02	0.29	-1.80
119	AAI64051.1	F11 receptor	f11r.1	2.21E-02	0.29	-1.80
120	AAH54622.1	Annexin A4	anxa4	2.75E-06	0.29	-1.79
121	AAH59566.1	Heat shock factor binding protein 1	hsbp1b	4.63E-04	0.29	-1.79
122	AAH95030.1	Zgc:112425	cirbpa	3.17E-03	0.29	-1.78

No.	Accesion	Description	Gene Symbol	p-value	Fold change	log_2 (FC)
123	XP_005161962.1	protein kinase C and casein kinase substrate in neurons 1a isoform X1	pacsin1a	5.82E-03	0.29	-1.78
124	AAB05403.1	bA1 globin	ba1l	3.52E-05	0.29	-1.78
125	CAM16712.1	novel protein similar to vertebrate skeletal alpha-actin 1 (ACTA1, zgc:86725)	actc1c	1.26E-03	0.29	-1.77
126	NP_998507.1	aromatic-L-amino-acid decarboxylase	ddc	7.00E-05	0.29	-1.76
127	AAH56783.1	Zgc:63561	cisd1	4.17E-03	0.30	-1.75
128	AAH95636.1	Zgc:92635	tceb1b	1.18E-03	0.30	-1.75
129	AAH96883.1	Si:dkey-276i5.1 protein, partial	gars	1.33E-02	0.30	-1.74
130	NP_998458.1	serine/threonine-protein phosphatase 2A catalytic subunit beta isoform	ppp2cb	1.31E-04	0.30	-1.73
131	XP_005163651.1	elongation factor-1, delta, a isoform X5	eef1da	8.55E-03	0.30	-1.73
132	AAI65689.1	Rbm39a protein	rbm39a	6.71E-03	0.30	-1.73
133	AAH93295.1	Calpain 2, (m/II) large subunit, like	capn2l	4.55E-03	0.31	-1.71
134	Q58EB4.1	RecName: Full=3-hydroxyisobutyryl-CoA hydrolase, mitochondrial; AltName: Full=3-hydroxyisobutyryl-coenzyme A hydrolase; Short=HIB-CoA hydrolase; Short=HIBYL-CoA-H; Flags: Precursor	hibch	6.88E-06	0.31	-1.69
135	XP_005160491.1	secernin-2 isoform X1	scrn2	1.68E-02	0.31	-1.67
136	NP_001007792.1	crystallin, gamma M4	crygm4	5.86E-04	0.32	-1.66
137	AAI63932.1	Solute carrier family 4, anion exchanger, member 1	slc4a1a	1.74E-03	0.32	-1.66
138	AAH65633.1	Zgc:77262	zgc:77262	9.15E-03	0.32	-1.65
139	AAU85359.1	interferon regulatory factor 6	irf6	7.29E-05	0.32	-1.64

No.	Accesion	Description	Gene Symbol	p-value	Fold change	log_2 (FC)
140	XP_009296840.2	E3 ubiquitin-protein ligase RNF31	LOC100334178	9.81E-05	0.32	-1.62
141	AAI64979.1	Crygs3 protein	crygs3	2.20E-06	0.33	-1.62
142	AAH95585.1	Angiotensinogen	agt	2.31E-06	0.33	-1.60
143	AAH66618.1	Chloride intracellular channel 1	clic1	3.87E-05	0.33	-1.60
144	XP_017209012.1	60S ribosomal protein L10 isoform X1	rpl10	2.79E-04	0.33	-1.60
145	XP_005168739.1	adenylate kinase isoenzyme 1 isoform X1	ak1	4.56E-04	0.33	-1.60
146	NP_001038796.1	uncharacterized protein LOC724056	alox5b.2	1.25E-02	0.33	-1.59
147	AAH62838.1	Hydroxysteroid dehydrogenase like 2	hsdl2	8.03E-05	0.33	-1.59
148	AAH59449.1	Retinaldehyde binding protein 1a	rlbp1a	1.00E-02	0.33	-1.58
149	AAI25915.1	Zgc:153928	cd99	4.09E-04	0.33	-1.58
150	AAI24716.1	Unknown (protein for IMAGE:7919542), partial	LOC100005356	2.07E-05	0.34	-1.58
151	NP_001182713.2	selenoprotein E precursor	selenoe	2.44E-02	0.34	-1.57
152	XP_691535.5	complexin-1	LOC563082	3.34E-03	0.34	-1.56
153	AAI52694.1	Ribosomal protein S20	rps20	3.32E-04	0.34	-1.55
154	AAI55096.1	Ribosomal protein L15	rpl15	2.28E-03	0.34	-1.55
155	AAH64286.1	Cathepsin C	ctsc	3.58E-04	0.34	-1.55
156	XP_005172121.1	galectin-1 isoform X1	lgals2b	4.12E-03	0.34	-1.54
157	AAI54042.1	Si:ch211-234p6.12 protein	crp3	1.49E-04	0.34	-1.54

No.	Accesion	Description	Gene Symbol	p-value	Fold change	log_2 (FC)
158	XP_021334401.1	ATP-dependent RNA helicase DDX3X isoform X1	ddx3a	9.74E-05	0.35	-1.53
159	NP_001103866.1	sorting nexin-10B	snx10b	1.50E-04	0.35	-1.53
160	NP_001007365.1	coatomer subunit epsilon	cope	3.58E-04	0.35	-1.52
161	AAH71527.1	Phosphoribosylaminoimidazole carboxylase, phosphoribosylaminoimidazole succinocarboxamide synthetase	paics	1.28E-02	0.35	-1.51
162	XP_005159454.1	ubiquitin-associated protein 2-like isoform X1	ubap2l	7.14E-06	0.35	-1.50
163	XP_021325780.1	aminoacyl tRNA synthase complex-interacting multifunctional protein 2 isoform X1	aimp2	8.01E-05	0.35	-1.50
164	NP_851847.1	60 kDa heat shock protein, mitochondrial	hspd1	6.49E-04	0.35	-1.50
165	XP_017206442.1	eukaryotic translation initiation factor 3 subunit K isoform X1	eif3k	3.20E-05	0.36	-1.49
166	AAH95773.1	Methylmalonyl CoA epimerase	mcee	2.73E-02	0.36	-1.49
167	AAH92978.1	PDZ and LIM domain 1 (elfin)	pdlim1	4.26E-04	0.36	-1.48
168	AAI15109.1	Zgc:109868	krt92	1.97E-03	0.36	-1.48
169	AAI55574.1	LOC792623 protein, partial	dusp27	1.06E-02	0.36	-1.48
170	XP_021321971.1	tripartite motif-containing protein 59 isoform X1	trim59	1.72E-04	0.36	-1.48
171	NP_999976.1	protein phosphatase 1, catalytic subunit, alpha	ppp1caa	2.02E-02	0.36	-1.47
172	XP_017206451.1	A-kinase anchor protein 1, mitochondrial isoform X1	akap1b	1.11E-03	0.36	-1.46
173	AAI54823.1	Gapdhs protein	gapdhs	4.40E-05	0.37	-1.44
174	AAH46057.1	RNA binding motif protein 4.1	rbm4.1	1.77E-03	0.37	-1.43
175	NP_001007386.1	chloride intracellular channel protein 5	clic5a	4.58E-03	0.37	-1.43

No.	Accesion	Description	Gene Symbol	p-value	Fold change	log_2 (FC)
176	AAG27059.1	Na+/K+ ATPase alpha subunit isoform 7	atp1a1b	3.07E-04	0.37	-1.42
177	AAH76451.1	Zgc:91854	blvrb	7.92E-05	0.37	-1.42
178	XP_009290394.1	uncharacterized protein si:dkeyp-77h1.4	si:dkeyp-77h1.4	1.23E-03	0.38	-1.41
179	NP_942096.1	creatine kinase U-type, mitochondrial	ckmt1	2.66E-06	0.38	-1.40
180	AAH44429.1	Zgc:55573	eloa	1.35E-03	0.38	-1.40
181	AAH59509.1	Zgc:73149	rpl23	1.47E-04	0.38	-1.40
182	AAH65970.1	Heat shock protein 4	hspa4b	4.61E-04	0.38	-1.39
183	AAZ94304.1	four and half LIM domains protein 2 isoform a	fhl2a	3.28E-03	0.38	-1.38
184	AAZ08576.1	fatty acid binding protein 1b	fabp1b.1	8.88E-06	0.38	-1.38
185	XP_009303852.2	unconventional myosin-XVIIIa isoform X1	myo18aa	9.88E-05	0.38	-1.38
186	XP_009295920.3	TBC1 domain family member 24 isoform X1	tbc1d24	4.60E-04	0.39	-1.38
187	XP_017207094.1	synaptosomal-associated protein 23 isoform X1	snap23.1	1.91E-02	0.39	-1.37
188	O42363.1	RecName: Full=Apolipoprotein A-I; Short=Apo-AI; Short=ApoA-I; AltName: Full=Apolipoprotein A1; Contains: RecName: Full=Proapolipoprotein A-I; Short=ProapoA-I; Flags: Precursor	apoa1a	2.11E-05	0.39	-1.37
189	CAQ14532.1	calcyclin binding protein	cacybp	6.18E-04	0.39	-1.37
190	AAH53267.1	Fructose-1,6-bisphosphatase 1b	fbp1b	6.60E-05	0.39	-1.37
191	AAI25893.1	Gsna protein, partial	gsna	1.68E-03	0.39	-1.34
192	AAH52111.1	Zinc finger protein 259	zpr1	6.55E-06	0.39	-1.34
193	Q8JFV8.1	RecName: Full=Synaptic vesicle membrane protein VAT-1 homolog	vat1	1.12E-02	0.40	-1.34

No.	Accesion	Description	Gene Symbol	p-value	Fold change	log_2 (FC)
194	NP_957471.1	programmed cell death protein 5	pdcd5	8.30E-04	0.40	-1.34
195	ABB89039.1	thioredoxin-like protein	txndc12	4.28E-04	0.40	-1.34
196	NP_001013277.3	serine (or cysteine) proteinase inhibitor, clade A (alpha-1 antiproteinase, antitrypsin), member 1, like precursor	serpina1l	2.23E-03	0.40	-1.32
197	AAP93667.1	embryonic globin beta e3, partial	hbbe3	9.88E-03	0.40	-1.32
198	AAH49040.1	Zgc:56530	cst14a.2	5.90E-04	0.40	-1.32
199	AAH83303.1	Adaptor-related protein complex 3, sigma 1 subunit	ap3s1	4.21E-03	0.40	-1.31
200	XP_009303756.1	uncharacterized protein LOC103911757	LOC103911757	6.52E-03	0.40	-1.31
201	NP_956468.2	uridine 5'-monophosphate synthase	umps	6.03E-03	0.40	-1.31
202	XP_002663594.2	periostin	postna	3.77E-04	0.40	-1.31
203	NP_001313311.1	niban-like	fam129bb	1.64E-04	0.40	-1.30
204	AAH62527.1	Glycine N-methyltransferase	gnmt	3.30E-05	0.41	-1.29
205	NP_001077321.1	uncharacterized protein LOC570464 precursor	wu:fu71h07	3.14E-03	0.41	-1.29
206	XP_021335783.1	dihydropyrimidinase-related protein 4 isoform X1	dpysl4	8.50E-04	0.41	-1.29
207	NP_001121673.1	microtubule-associated protein 1B	map1b	3.34E-02	0.41	-1.29
208	AAH58315.1	Eukaryotic translation elongation factor 1 gamma	eef1g	4.26E-04	0.41	-1.28
209	NP_998804.1	non-muscle cofilin 1	cfl1l	3.54E-04	0.41	-1.28
210	AAI07984.1	Sept2 protein, partial	sept2	2.45E-03	0.41	-1.27
211	AAH85467.1	Zgc:101897	gsto2	9.64E-04	0.41	-1.27

No.	Accesion	Description	Gene Symbol	p-value	Fold change	log_2 (FC)
212	AAI54308.1	Tyrosine 3-monooxygenase/tryptophan 5-monooxygenase activation protein, theta polypeptide a	ywhaqa	4.76E-04	0.41	-1.27
213	XP_005159012.1	uncharacterized protein LOC559822 isoform X1	zgc:162184	7.88E-03	0.42	-1.27
214	CAC19188.1	trypsin, partial	prss1	7.01E-05	0.42	-1.27
215	AAG30273.1	Na+/K+ ATPase beta subunit isoform 1b	atp1b1b	5.97E-05	0.42	-1.26
216	AAI53392.1	Zgc:123103	zgc:123103	3.14E-05	0.42	-1.25
217	AAT64103.1	reticulon 1-a1	rtn1b	7.70E-03	0.42	-1.25
218	AAH91851.1	Aldh16a1 protein, partial	aldh16a1	1.14E-05	0.43	-1.23
219	AAI53542.1	Serpin peptidase inhibitor, clade A (alpha-1 antiproteinase, antitrypsin), member 7	serpina7	1.36E-04	0.43	-1.23
220	XP_002662785.1	natterin-like protein	LOC564481	4.51E-02	0.43	-1.23
221	AAH71363.1	Glycogenin, like	gyg1b	1.01E-03	0.43	-1.22
222	XP_005157462.1	neural cell adhesion molecule 1b isoform X1	ncam1b	4.27E-02	0.43	-1.22
223	AAH81658.1	Protein phosphatase 2 (formerly 2A), regulatory subunit A, beta isoform	ppp2r1bb	4.71E-02	0.43	-1.22
224	AAH59684.1	Zgc:73375	ndufb6	1.30E-02	0.43	-1.21
225	NP_997926.1	ictacalcin	icn	1.37E-02	0.44	-1.20
226	NP_957044.1	40S ribosomal protein S19	rps19	2.84E-04	0.44	-1.18
227	XP_017206833.1	uridine phosphorylase 1 isoform X1	upp1	1.73E-04	0.44	-1.18
228	AAH66678.1	Ribophorin II	rpn2	4.70E-03	0.44	-1.18
229	NP_001299846.1	serine/threonine-protein phosphatase 2A 65 kDa regulatory subunit A beta isoform	ppp2r1ba	1.42E-04	0.45	-1.17

No.	Accesion	Description	Gene Symbol	p-value	Fold change	log_2 (FC)
230	AAK33032.1	Na+/K+ ATPase alpha2 subunit	atp1a2a	3.67E-06	0.45	-1.16
231	AAH76347.1	Peroxiredoxin 2	prdx2	2.59E-05	0.45	-1.16
232	AAH65874.1	Eif3s2 protein	eif3i	3.09E-03	0.45	-1.15
233	AAU85774.1	gammaM2b-crystallin	crygm2b	6.24E-05	0.45	-1.15
234	NP_001002657.2	ubiquinol-cytochrome c reductase core protein II	uqcrc2a	1.60E-04	0.45	-1.15
235	AAI33833.1	Neuraminidase 1	neu1	5.61E-05	0.45	-1.14
236	NP_001124122.1	uncharacterized protein LOC100170815	zgc:193598	3.54E-03	0.45	-1.14
237	NP_001303825.1	guanylate kinase isoform 1	guk1a	3.97E-03	0.45	-1.14
238	XP_009294646.1	complement factor H like 4 isoform X1	cfhl4	1.63E-02	0.45	-1.14
239	XP_021329305.1	troponin C, skeletal muscle	si:rp71-17i16.4	3.30E-04	0.45	-1.14
240	AAI17589.1	Topoisomerase (DNA) I, like	top1l	4.68E-03	0.45	-1.14
241	AAU14809.1	fibronectin 1b	fn1b	3.07E-03	0.46	-1.14
242	AAI65889.1	Zgc:92732 protein	gcshb	6.84E-05	0.46	-1.13
243	AAP93851.1	intestinal fatty acid binding protein 2	fabp2	1.20E-02	0.46	-1.13
244	NP_999936.1	epidermal retinol dehydrogenase 2	sdr16c5b	3.16E-03	0.46	-1.13
245	XP_009289535.1	neutral alpha-glucosidase AB	ganab	1.30E-03	0.46	-1.13
246	AAH83504.1	Heat shock protein 9	hspa9	6.92E-03	0.46	-1.12
247	XP_706416.1	chromosomal protein D1	si:ch211-288g17.3	2.45E-05	0.46	-1.10

No.	Accesion	Description	Gene Symbol	p-value	Fold change	log_2 (FC)
248	AAG27058.1	Na+/K+ ATPase alpha subunit isoform 6	atp1a3b	2.41E-04	0.47	-1.10
249	XP_021324619.1	cingulin-like	LOC101884022	1.34E-03	0.47	-1.10
250	AAH74079.1	Zgc:91835	dbnla	2.25E-03	0.47	-1.10
251	NP_001007391.1	3-hydroxyanthranilate 3,4-dioxygenase	haao	3.64E-04	0.47	-1.10
252	XP_021329525.1	microtubule-associated protein 1B isoform X1	map1ab	4.60E-03	0.47	-1.10
253	Q7ZU99.1	RecName: Full=Transitional endoplasmic reticulum ATPase; Short=TER ATPase; AltName: Full=Protein CDC48; AltName: Full=Valosin-containing protein; Short=VCP	vcp	1.04E-04	0.47	-1.10
254	NP_001077046.1	RNA polymerase-associated protein RTF1 homolog	rtf1	1.67E-04	0.47	-1.09
255	AAH85625.1	Phenylalanine-tRNA synthetase-like	farsb	2.93E-03	0.47	-1.09
256	NP_999881.1	heat shock protein 4a	hspa4a	4.97E-03	0.47	-1.08
257	XP_005156863.1	40S ribosomal protein S24 isoform X1	rps24	6.43E-04	0.47	-1.08
258	AAO86703.1	glutathione peroxidase, partial	gpx1a	5.38E-04	0.48	-1.07
259	NP_001186660.1	glutamyl aminopeptidase	enpep	4.20E-04	0.48	-1.07
260	NP_991263.1	cofilin-2	cfl2	3.84E-05	0.48	-1.07
261	NP_957046.1	40S ribosomal protein S7	rps7	2.72E-04	0.48	-1.06
262	AAI64059.1	Fhla protein	fhl1a	5.10E-04	0.48	-1.06
263	XP_021331635.1	MOB kinase activator 1A isoform X1	mob1a	2.01E-03	0.48	-1.06
264	CAQ14651.1	proteasome (prosome, macropain) subunit, beta type, 5	psmb5	1.30E-02	0.48	-1.06

No.	Accesion	Description	Gene Symbol	p-value	Fold change	log_2 (FC)
265	XP_021332461.1	obg-like ATPase 1 isoform X1	ola1	7.96E-05	0.48	-1.06
266	Q6NWE0.1	RecName: Full=Ester hydrolase C11orf54 homolog	zgc:85789	2.03E-03	0.48	-1.06
267	XP_005171384.1	microtubule-associated protein 1S	map1sb	1.06E-02	0.48	-1.06
268	NP_001129995.1	slow myosin heavy chain 3	smyhc3	1.03E-04	0.48	-1.05
269	ABG35925.1	SULT2 ST3	sult2st3	1.75E-03	0.48	-1.05
270	AAH55155.1	Aldehyde dehydrogenase 4 family, member A1	aldh4a1	3.16E-03	0.48	-1.05
271	XP_021334842.1	talin-1 isoform X1	tln1	8.86E-06	0.48	-1.05
272	NP_001315318.1	phosphofructokinase, liver b	pfklb	1.44E-02	0.49	-1.04
273	AAH62860.1	Chloride intracellular channel a	clic3	1.27E-02	0.49	-1.03
274	XP_017212317.1	phosphorylase, glycogen, muscle b isoform X1	pygmb	5.05E-04	0.49	-1.03
275	NP_001004529.1	enoyl-CoA hydratase, mitochondrial	echs1	4.34E-02	0.49	-1.03
276	NP_001013573.3	amine oxidase copper containing 2	aoc2	3.14E-03	0.49	-1.02
277	AAK97853.1	alcohol dehydrogenase	adh8a	4.17E-04	0.49	-1.02
278	AAH77128.1	Homer homolog 1 (Drosophila)	homer1b	2.51E-02	0.50	-1.01
279	NP_001278815.1	apolipoprotein C-I isoform 1 precursor	apoc1	2.82E-04	0.50	-1.01
280	AAI07982.1	Calponin 3, acidic b	cnn3b	1.69E-05	0.50	-1.01
281	AAH66531.1	Scinderin like b	scinlb	7.99E-03	0.50	-1.00
282	NP_001280633.1	complement C1q-like protein 4-like precursor	cbln11	5.20E-03	0.50	-1.00
283	XP_005171556.1	uncharacterized protein LOC100007431 isoform X2	zgc:172051	3.07E-04	0.50	-1.00

No.	Accesion	Description	Gene Symbol	p-value	Fold change	log_2 (FC)
284	NP_991230.1	small nuclear ribonucleoprotein polypeptides B and B1	snrpb	5.20E-03	0.50	-1.00
285	NP_001025345.2	DNA ligase 3	lig3	1.09E-03	0.50	-1.00
286	AAH92763.1	Stathmin 1/oncoprotein 18	stmn1b	1.87E-03	2.00	1.00
287	AAI52656.1	Arrestin 3, retinal (X-arrestin)	arr3b	9.12E-03	2.03	1.02
288	AAH65652.1	Zgc:56488	ddrgk1	3.67E-04	2.04	1.03
289	XP_001335256.1	uncharacterized protein si:dkey-30j10.5	si:dkey-30j10.5	1.94E-03	2.05	1.03
290	XP_021330897.1	filamin-C isoform X1	flncb	4.37E-03	2.05	1.03
291	AAI52212.1	Chchd2l protein	chchd2	6.30E-04	2.06	1.04
292	AAH58045.1	Collagen, type I, alpha 3	col1a1b	9.08E-05	2.07	1.05
293	XP_005165704.1	ankyrin 1, erythrocytic a isoform X20	ank1a	2.19E-03	2.09	1.07
294	Q503Q1.2	RecName: Full=Mitochondria-eating protein; AltName: Full=Spermatogenesis-associated protein 18	spata18	4.76E-04	2.10	1.07
295	AAH44559.1	DnaJ (Hsp40) homolog, subfamily B, member 11	dnajb11	1.68E-02	2.17	1.12
296	XP_001338671.2	caldesmon, smooth muscle-like isoform X1	si: ch211-223l2.4	1.04E-02	2.19	1.13
297	BAK26516.1	S100A1 protein	s100a1	6.61E-04	2.20	1.14
298	AAH95812.1	Zgc:112421	anxa13l	3.89E-04	2.20	1.14
299	AAP33154.1	fast troponin T isoform b	tnnt3b	3.68E-05	2.21	1.14
300	XP_021326297.1	mucin-2 isoform X1	muc5.1	9.74E-04	2.22	1.15
301	NP_899181.1	piwi-like protein 1	piwil1	1.83E-05	2.23	1.16

No.	Accesion	Description	Gene Symbol	p-value	Fold change	log_2 (FC)
302	XP_021323007.1	titin isoform X1	si:ch211-266g18.10	3.33E-04	2.24	1.16
303	XP_003201179.1	U6 snRNA-associated Sm-like protein LSm3	lsm3	9.83E-06	2.27	1.18
304	XP_021335602.1	peroxisome proliferator-activated receptor gamma coactivator-related protein 1-like	LOC110440113	6.21E-04	2.31	1.21
305	XP_009295366.1	FYVE and coiled-coil domain-containing protein 1-like isoform X1	fyco1a	3.93E-04	2.32	1.21
306	AAH45423.1	Zgc:55673	lsm14b	2.82E-05	2.33	1.22
307	XP_005162222.1	complement receptor-like protein isoform X1	rca2.1	4.41E-02	2.35	1.23
308	ABB29996.1	V-FBPL precursor	si:ch1073-376c22.1	3.29E-02	2.39	1.26
309	AAH49512.1	Wu:fi12b10 protein, partial	si:dkey-37o8.1	4.62E-05	2.43	1.28
310	XP_687541.4	poly(ADP-ribose) glycohydrolase	parga	1.45E-04	2.44	1.29
311	XP_683261.4	protein PAT1 homolog 2	si:ch211-103b1.2	1.57E-04	2.45	1.30
312	XP_017210396.1	pregnancy zone protein	zgc:171426	2.26E-03	2.46	1.30
313	AAH66496.1	Shmt1 protein	shmt1	3.83E-02	2.47	1.30
314	AAH51625.1	Transcription elongation factor B (SIII), polypeptide 3	calcoco1b	5.97E-04	2.51	1.33
315	Q7SXV9.1	RecName: Full=Calumenin-B; Flags: Precursor	calub	7.15E-03	2.53	1.34
316	XP_021332540.1	eukaryotic translation initiation factor 4E transporter isoform X1	eif4enif1	9.05E-04	2.53	1.34
317	NP_001096141.1	vitellogenin 7 precursor	vtg7	2.77E-06	2.56	1.35
318	NP_001280600.1	actinoporin-like protein	apnl	3.92E-03	2.57	1.36

No.	Accesion	Description	Gene Symbol	p-value	Fold change	$\log_2$ (FC)
319	AAI35069.1	Krt1-19d protein, partial	krt1-19d	6.83E-04	2.67	1.42
320	NP_957511.2	nucleolar protein 56 isoform 1	nop56	5.24E-04	2.72	1.44
321	NP_571316.1	complement component bfb precursor	bfb	1.76E-02	2.72	1.45
322	AAI46704.1	Zgc:165344 protein	mybphb	5.90E-03	2.75	1.46
323	AAI15327.1	Cryl1 protein, partial	cryl1	2.99E-02	2.78	1.48
324	XP_021326058.1	obscurin	obscnb	1.62E-03	2.81	1.49
325	AAI65266.1	Zgc:110380 protein, partial	histh1l	2.62E-02	2.87	1.52
326	AAI60653.1	Coatomer protein complex, subunit beta 2	copb2	2.52E-03	2.93	1.55
327	AAI33967.1	Si:dkey-238c7.16 protein	si:dkey-238c7.16	3.78E-02	3.01	1.59
328	NP_571843.1	claudin i	cldni	2.68E-03	3.03	1.60
329	NP_001315343.1	noelin isoform 1	olfm1b	6.80E-04	3.03	1.60
330	NP_001093467.1	probable global transcription activator SNF2L1	smarca1	4.40E-03	3.07	1.62
331	AAI64525.1	Zgc:153629 protein	krt94	1.07E-03	3.16	1.66
332	Q6P0D0.2	RecName: Full=Protein quaking-A; Short=zqk	qkia	1.43E-03	3.18	1.67
333	NP_001012372.1	hepatoma-derived growth factor-related protein 3	hdgfl3	1.36E-02	3.26	1.70
334	XP_021326591.1	vitellogenin-like	LOC110438452	1.81E-04	3.29	1.72
335	AAI28876.1	S100u protein, partial	s100u	4.30E-05	3.63	1.86
336	NP_001077285.2	uncharacterized protein LOC553299	zgc:162509	1.96E-05	3.66	1.87

No.	Accesion	Description	Gene Symbol	p-value	Fold change	log_2 (FC)
337	XP_017206965.1	uncharacterized protein LOC100149015	LOC100149015	4.12E-04	3.82	1.93
338	XP_009301745.2	protein kinase C and casein kinase substrate in neurons protein 3 isoform X1	pacsin3	2.87E-03	3.94	1.98
339	XP_005171901.1	occludin isoform X1	oclnb	2.93E-02	4.14	2.05
340	NP_998472.1	ATP synthase-coupling factor 6, mitochondrial	atp5j	2.20E-03	4.22	2.08
341	AAI42778.1	LOC572200 protein, partial	LOC572200	1.53E-05	4.28	2.10
342	Q5PR67.2	RecName: Full=Eukaryotic translation initiation factor 3 subunit H-B; Short=eIF3h-B; AltName: Full=Eukaryotic translation initiation factor 3 subunit 3-B; AltName: Full=eIF-3-gamma-B; AltName: Full=eIF3 p40 subunit B	eif3hb	2.06E-04	4.36	2.12
343	XP_005171873.1	porphobilinogen deaminase isoform X1	hmbsa	3.20E-03	4.38	2.13
344	AAH97081.1	Vitellogenin 5	vtg5	2.79E-03	4.57	2.19
345	AAI51979.1	Zgc:171779 protein	zgc:171779	2.02E-02	4.63	2.21
346	XP_009305650.2	synaptopodin 2-like protein isoform X1	synpo2la	1.99E-02	4.64	2.21
347	AAH65640.1	Zgc:77282	eif4h	2.07E-03	4.74	2.24
348	NP_571132.1	probable ATP-dependent RNA helicase DDX4	ddx4	1.52E-02	5.09	2.35
349	AAI64432.1	Zgc:77734 protein	dbi	2.56E-03	5.21	2.38
350	XP_005163864.2	voltage-dependent L-type calcium channel subunit beta-1 isoform X1	cacnb1	1.45E-04	5.22	2.38
351	NP_001136064.1	leucine-rich PPR motif-containing protein, mitochondrial	lrpprc	2.06E-03	5.30	2.41
352	AAI50353.1	Si:dkey-208k4.2 protein	si:dkey-208k4.2	3.40E-04	5.39	2.43
353	XP_697108.5	sarcoplasmic/endoplasmic reticulum calcium ATPase 3 isoform X1	atp2a3	4.62E-04	5.55	2.47

No.	Accesion	Description	Gene Symbol	p-value	Fold change	log_2 (FC)
354	NP_001070742.1	uncharacterized protein LOC768128	cst14b.1	1.46E-05	5.62	2.49
355	AAQ54326.1	cellular retinol-binding protein type 1	rbp5	1.43E-02	6.48	2.70
356	NP_001296966.1	NADP-dependent malic enzyme	me1	2.20E-04	6.88	2.78
357	XP_017209059.1	breast carcinoma-amplified sequence 1 isoform X3	zgc:112994	1.74E-04	7.25	2.86
358	XP_009292473.1	insulin-like growth factor 2 mRNA-binding protein 3 isoform X1	igf2bp3	1.78E-04	7.46	2.90
359	XP_009302595.1	FK506-binding protein 15 isoform X1	si:ch73-199g24.2	8.97E-04	8.63	3.11
360	NP_001075216.2	vesicular integral-membrane protein VIP36 precursor	lman2	1.00E-03	8.90	3.15
361	XP_021326148.1	RNA-binding protein with multiple splicing 2 isoform X1	rbpms2a	1.07E-02	10.19	3.35
362	XP_685297.5	guanylate cyclase soluble subunit beta-2-like	gucy1b2	2.47E-03	11.19	3.48
363	NP_001038759.2	vitellogenin 4 precursor	vtg4	5.63E-06	12.25	3.61
364	AAQ63170.1	coatomer protein complex subunit alpha	copa	3.16E-04	14.91	3.90
365	NP_001038378.1	vitellogenin 2 isoform 1	vtg2	5.78E-08	26.15	4.71
366	AAI39547.1	Zgc:162209 protein	cdnf	4.99E-06	266.67	8.06
367	AAH65610.1	Fibrillarin	fbl	5.60E-06	266.67	8.06
368	XP_003199139.1	uncharacterized protein si:ch211-167b20.8 isoform X1	si:ch211-167b20.8	1.04E-05	266.67	8.06
369	NP_001098746.1	trifunctional enzyme subunit alpha, mitochondrial	hadhaa	7.32E-05	266.67	8.06
370	XP_687465.5	myoferlin	myofl	1.51E-04	266.67	8.06
371	AAI65166.1	Tkt protein	tktb	1.51E-04	266.67	8.06

No.	Accesion	Description	Gene Symbol	p-value	Fold change	log_2 (FC)
372	XP_005168648.1	protein kinase C and casein kinase substrate in neurons protein 2 isoform X1	pacsin2	1.78E-04	266.67	8.06
373	AAQ98010.1	cullin 3	cul3a	6.38E-04	266.67	8.06
374	AAH90800.1	LOC553309 protein, partial	fam169ab	3.10E-03	266.67	8.06
375	NP_001139070.1	uncharacterized protein LOC567396	cnn1a	1.56E-02	266.67	8.06
376	AAH47167.1	Trk-fused gene	tfg	1.96E-02	266.67	8.06

Figure 14. Venn diagram of biomarker proteins in each sample group.

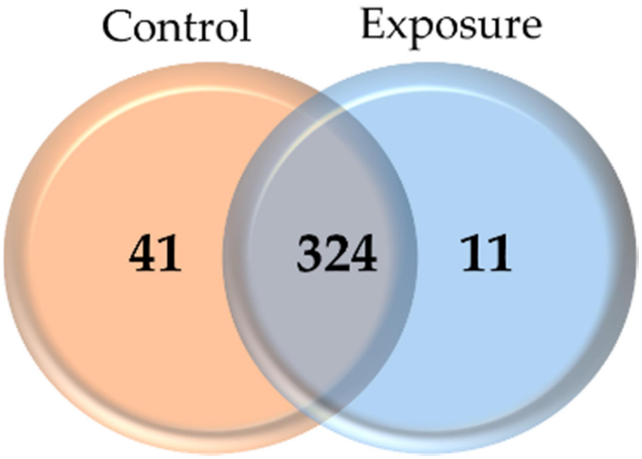
Control
Exposure
41
324
11

Figure 15. Gene ontology classification of biomarker proteins.

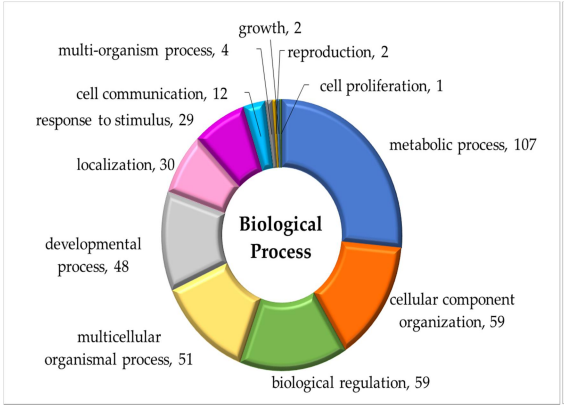
Biological Process
growth, 2
multi-organism process, 4
reproduction, 2
cell proliferation, 1
cell communication, 12
response to stimulus, 29
metabolic process, 107
localization, 30
developmental process, 48
cellular component organization, 59
multicellular organismal process, 51
biological regulation, 59

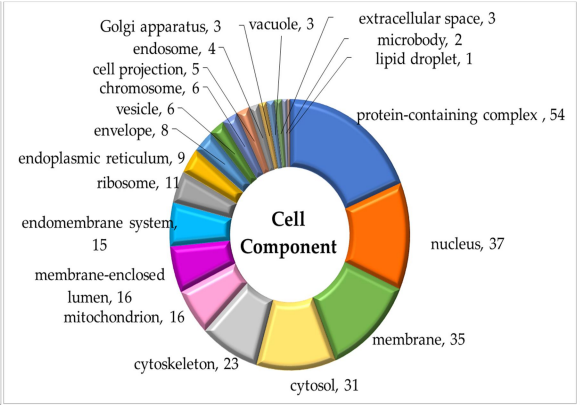
Cell Component
Golgi apparatus, 3
vacuole, 3
extracellular space, 3
endosome, 4
microbody, 2
lipid droplet, 1
cell projection, 5
chromosome, 6
protein-containing complex , 54
vesicle, 6
envelope, 8
endoplasmic reticulum, 9
ribosome, 11
endomembrane system, 15
nucleus, 37
membrane-enclosed lumen, 16
mitochondrion, 16
membrane, 35
cytoskeleton, 23
cytosol, 31

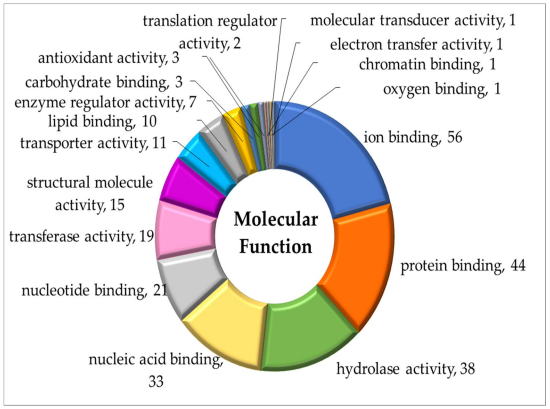
Molecular Function
translation regulator activity, 2
molecular transducer activity, 1
electron transfer activity, 1
antioxidant activity, 3
chromatin binding, 1
carbohydrate binding, 3
oxygen binding, 1
enzyme regulator activity, 7
lipid binding, 10
ion binding, 56
transporter activity, 11
structural molecule activity, 15
transferase activity, 19
protein binding, 44
nucleotide binding, 21
nucleic acid binding, 33
hydrolase activity, 38

Metabolic pathway analysis from only proteomic biomarkers

Alteration of proteomic biomarkers identified by profiling with LC-Orbitrap-MS/MS makes it possible to predict changes in metabolism caused by PCP. WebGestalt (web-based gene set analysis toolkit), website that supports integrated proteomic data mining system, suggests significantly related metabolic pathways based on gene sets in various biological contexts (Zhang et al., 2005). Proteomic pathway analysis (Figure 16) was carried out using Webgestalt with the number of observed genes divided the number of expected genes from the gene list (GO or KEGG) in x-axis of graph (Lascorz et al., 2011). With 376 biomarkers, several pathways were identified such as adrenergic siganalling in cardiomyocytes, glycolysis et al. Especially, 10 proteins related to ribosome (*rpl10, rpl15, rpl23, rpl35a, rplp0, rps16, rps19, rps2, rps20, rps24*) were downlgulated in PCP high-exposure group compared to control group. This corresponds to the content of the discussion later. This analysis indicated the overall alteration of protein expression level in zebrafish when exposed to PCP, suggesting direction for comprehensive pathway analysis.

Figure 16. Summary of pathway analyses of only proteomic biomarkers in zebrafish exposed to PCP with WebGestalt.

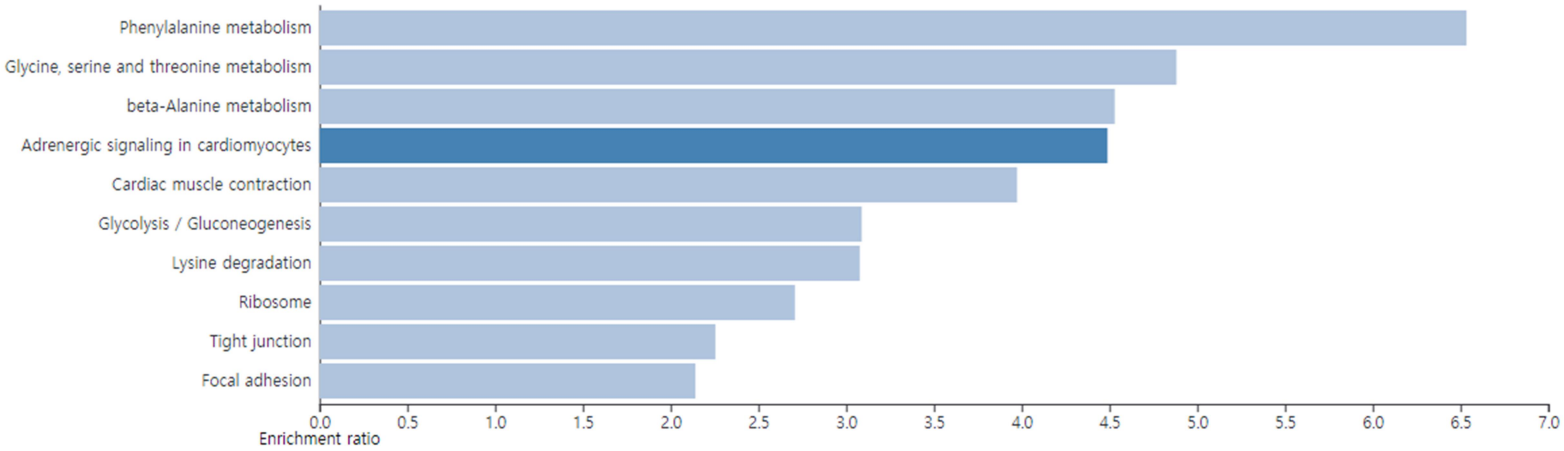
Phenylalanine metabolism
Glycine, serine and threonine metabolism
beta-Alanine metabolism
Adrenergic signaling in cardiomyocytes
Cardiac muscle contraction
Glycolysis / Gluconeogenesis
Lysine degradation
Ribosome
Tight junction
Focal adhesion
0.0
0.5
1.0
1.5
2.0
2.5
3.0
3.5
4.0
4.5
5.0
5.5
6.0
6.5
7.0
Enrichment ratio

Integrative pathway analysis of metabolomes and proteomes for toxic effect of PCP

The integration of multi-omics has gradually become an important approach to assess the potential toxic mechanism of xenobiotics and understand more comprehensively about the disease (Meng et al., 2014; Hasin et al., 2017). There was a direct correlation between the proteome and metabolome; because level of proteins exerted a powerful influence on the metabolic profile of a cell system and concentration of metabolites also might affect protein expression. Therefore, an integrated approach that combines proteomics and metabolomics data is a very powerful tool to provide a more comprehensive understanding of biological effects of potential toxicants. OmicsNet is a web-based tool for identifying complex biological networks by integrating various types of biomarkers (gene, proteins, and metabolites) (Akhmedov et al., 2017). The correlation between biomarkers of Mbx/Ptx and related metabolic pathways were predicted by OmicsNet (Figure 17). To elucidate interrelation between metabolite biomarker and proteome biomarker, integrative pathway analysis was performed using MetaboAnalyst 4.0 (Figure 18). Eight pathways identified include seven common pathways of metabolomics as in figure 8 (pentose phosphate pathway, pentose and glucuronate interconversions, taurine and hypotaurine metabolism, β-alanine metabolism, ascorbate and aldarate metabolism, alanine, aspartate and glutamate metabolism, and phenylalanine metabolism) and 1 pathway (nitrogen metabolism) from proteome biomarker. Of these results, seven pathways excluding nitrogen metabolism were selected as important pathways that could show significant change when exposed to PCP. Based on KEGG map, each selective pathway was interpreted in a schematic diagram to describe biochemical perturbation by PCP exposure (Figure 19)

Pentose phosphate pathway (PPP) is an essential pathway for synthesis of ribonucleotide, the basic building blocks of RNA (Kruger et al., 2003). During PCP exposure, the protein and metabolite indicated the inhibition of protein syntesis.

mRNA oxidation from oxidative stress may cause reduced protein expression (Shan et al., 2007). Inhibition of protein synthesis is very common phenomenon in diesease or exposure of toxic substance (Ennis et al., 1964, Ueno et al., 1973, Iglewski et al., 1975). Such persistent suppression of protein syntesis lead to cell death (Thilmann et al., 1986).

The levels of 3-hydroxypropionate(3-HP) and β-alanine in the β-alanine metabolism were increased by PCP exposure. Accumulation of 3-HP, small organic acid molecule, could cause acid toxicity in living organisms, and anions would interfere with enzyme (Warnecke et al., 2005, Chun et al., 2014). Moreover, 3- HP is suggested as a toxic metabolite by inhibiting the chorismate and threonine super-pathways (Warnecke et al., 2010). Excess β-alanine could also be toxic in living organisms. Administration of β-alanine would inhibit several enzymes like pyruvate kinase and superoxide dismustase activity, resulting in oxidative stress (Gemelli et al., 2013; Shetewy et al., 2016). It is estimated that the activity of proteins(aldh16a1 and aoc2) related to synthesize these metabolites may be reduced to prevent this toxic effect. In addition, there was a defect of echs1 and hibch gene expression in β-alanine metabolism, in this study. The impairment of echs1 and hibch gene expression caused disorders of energy production (Peters et al., 2014; Marti-Sanchez et al., 2020), and could affect neurological injury. PCP disrupted ATP synthesis as an uncoupling agent. PCP exposure has had a serious impact on immune defense by reducing the amount of ATP in human natural killer (NK) cells that perform tumor killing functions (Nnodu et al., 2008). This uncoupling agent increased mitochondrial respiration and decreased level of ATP (Buffa et al., 1963; Whitley et al., 1970). Moreover, decreased expression of echs1 and hibch genes has been known induce Leigh syndrome, a central nervous system injury disease (Ferdinandusse et al., 2013; Peters et al., 2015).

In the alanine, aspartate, and glutamate metabolism, N-acetyl aspartate (NAA) was reduced after PCP exposure. Leigh syndrome, a central nervous system

damage mentioned above, corresponds to the result of a decrease in NAA (Ruhoy et al., 2014). Most of NAA is found within the nervous system and it is used as a marker of neuronal integrity (Birken et al., 1989). The concentration of NAA is decreased depending on the degree of brain damage and impact on other metabolism like protein acetylation (Moffett et al., 2013). The loss of NAA is induced in the posttraumatic stress disorder with hippocampal abnormalities (Schuff et al., 2001; Ham et al., 2007). These studies support our findings that PCP may have been adverse neurological effects in living organisms.

With respect to phenylalanine metabolism, overall metabolite and protein expression is reduced in PCP exposured group. Alteration of tyrosine is used as a indicator of nitrosative and oxidative stress, because it is one of the susceptible metabolites to oxidative by ROS (Ali et al., 2004; Folkes et al., 2011). Therefore, this pathway may indicates that zebrafish exposed to PCP was injured by oxidative stress. It was also confirmed that oxidative stress in cells was induced when exposed to PCP by the result of measuring ROS and MDA. Oxidative stress contributes to carcinogenesis include modulation of gene expression and induction of genetic modifications (Mates et al., 2012). The effect of PCP-induced oxidative stress in causing cancer has been measured in the study of mice with change of cell proliferation and NAD(P) (Umemura et al., 2006). In addition, PCP exposure in human neuronal cells lead to apoptosis and necrosis by oxidative stress and reduce mitochondrial membrane potential (Fraser et al., 2019).

A defense system against the toxicity of PCP has also appeared and has been activated in zebrafish. To equip with adequate antioxidant defense and combat cancer, zebrafish exposed to PCP has significant alteration in taurine metabolism against control group. The level of taurine improved depending on the concentration of PCP. Taurine induces cell apoptosis against human colon cancer cell and its mechanism is already studied (Zhang et al., 2014). Moreover, taurine is the useful antioxidant to disrupt the increase of ROS in tumors, leading to delay of

the development of cancer (Das et al., 2009; Mates et al., 2012). MR spectroscopy revealed elevation of taurine and reduction of NAA in cerebral juvenile xanthogranuloma (Matsubara et al., 2016). These mean that increased taurine protect cells from oxidative stress leading to cytotoxicity as an effective antioxidant and treat the cancer in the zebrafish exposed to PCP.

When PCP is exposed, it is assumed that ascorbate and aldarate metabolism, pentose and glucuronate interconversion pathways have also been altered for defensive mechanism. Glucuronic acid acted as a significant molecule in the detoxification capacity of the liver by conjugating with toxic substances to form hydrophilic substances easily excreted in the urine (Muting et al., 1988; Sun et al., 2018). Moreover, increasing amount of glucuronate indicates that the body was stimulated to release more ascorbate to inhibit inflammatory reaction (Bernotti et al., 2003; Yao et al., 2015). In addition, better survival was proved for cancer patients via ascorbate and aldarate pathways (Xie et al., 2018). PCP, a toxic substance, can be decomposed through the Ascorbic acid-persulfate system (Cao et al., 2019). For these reasons, it is thought that the defense system against toxicity of PCP may be activated in zebrafish.

Figure 17. 2D visualized network schematics of metabolite-protein interaction using OmicsNet. The blue line in right figure represents the 7 metabolic pathways selected by biomarkers of Mbx/Ptx

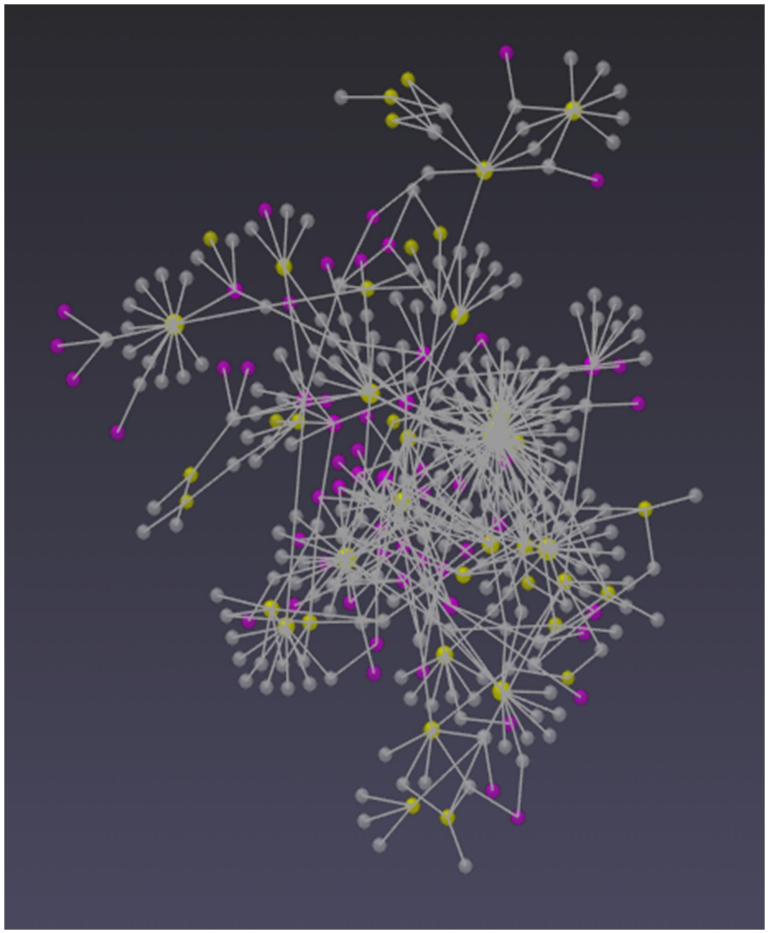

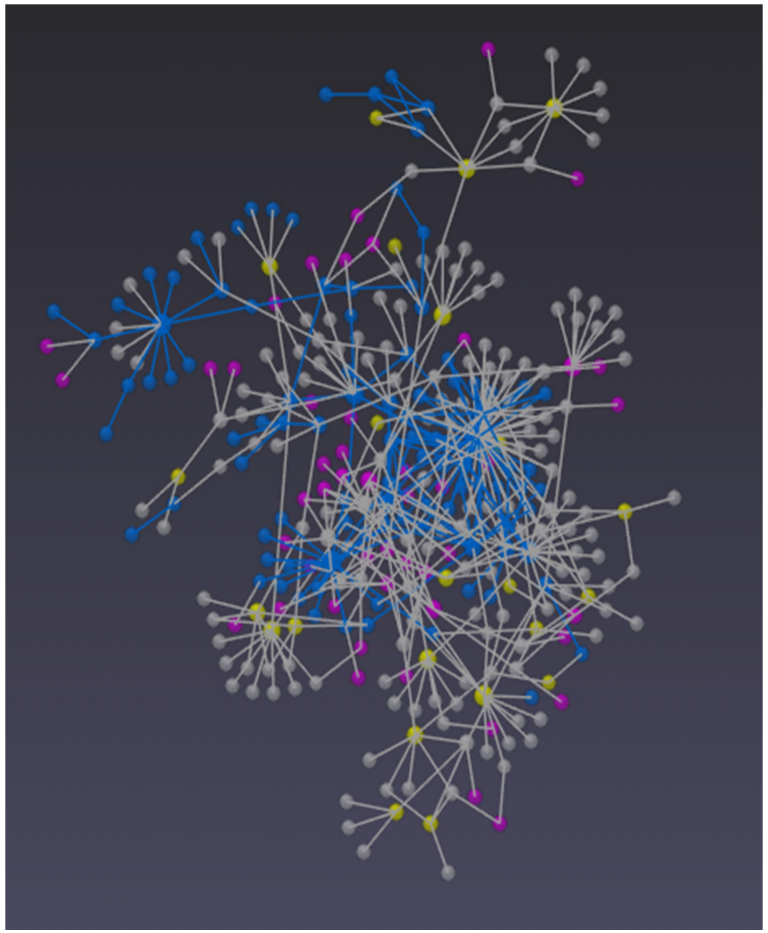

Figure 18. Integrative metabolomic and proteomic pathway analysis plot generated with metabolomic/proteomic biomarkers.

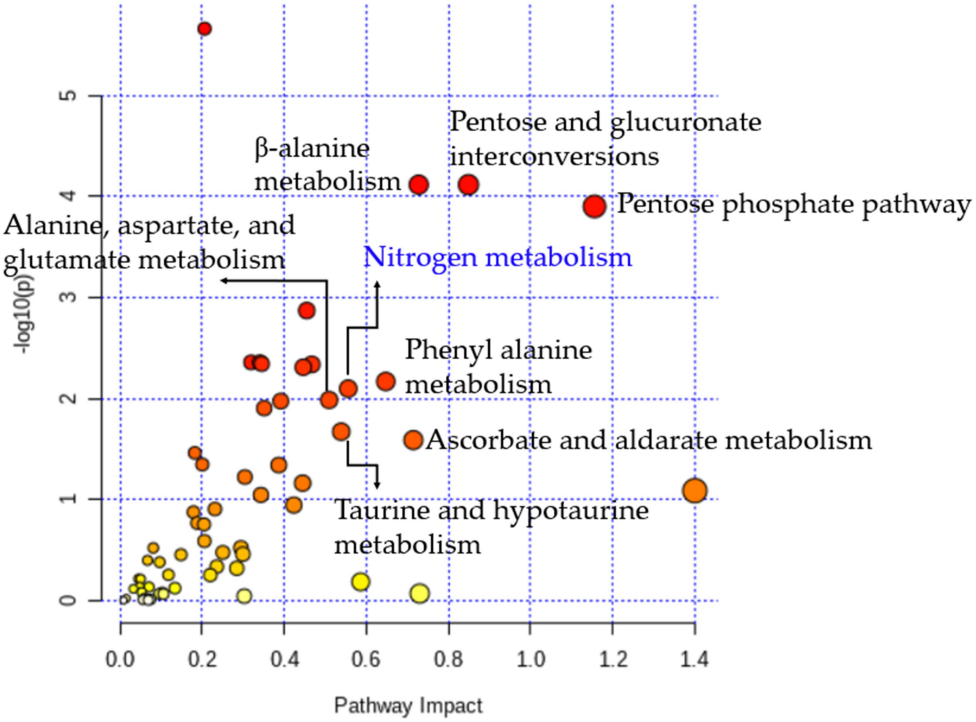
Pentose and glucuronate interconversions
β-alanine metabolism
Pentose phosphate pathway
Alanine, aspartate, and glutamate metabolism
Nitrogen metabolism
Phenyl alanine metabolism
Ascorbate and aldarate metabolism
Taurine and hypotaurine metabolism
-log10(p)
Pathway Impact
0
1
2
3
4
5
0.0
0.2
0.4
0.6
0.8
1.0
1.2
1.4

Figure 19. Predicted integrative network of metabolomes and proteomes altered by PCP exposure (* for $p < 0.05$, and ** for $p < 0.005$). The colors of red, green, and blue represent the control group, low exposure group (13 μg/L) and high exposure group (130 μg/L), respectively. The color of box represents group of each metabolomes: Red (increased metabolite biomarker), Blue (decreased metabolite biomarker), Black (detected metabolite, but not biomarker), and Gray (predicted metabolite related to gene expression).

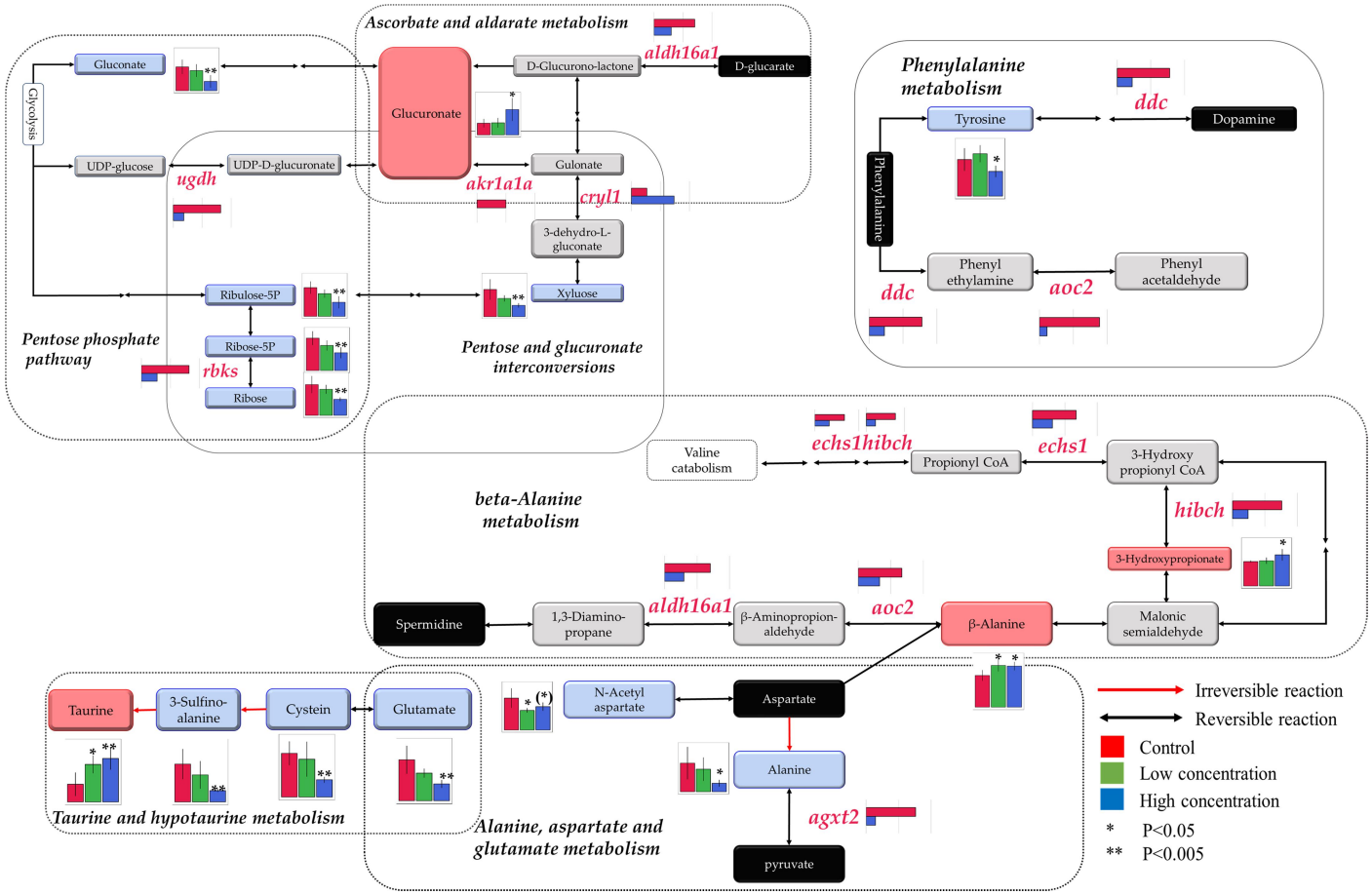
Ascorbate and aldarate metabolism
Gluconate
Glycolysis
UDP-glucose
UDP-D-glucuronate
ugdh
Glucuronate
D-Glucurono-lactone
aldh16a1
D-glucarate
Gulonate
akr1a1a
cryl1
3-dehydro-L-gluconate
Xyluose
Ribulose-5P
Ribose-5P
Ribose
rbks
Pentose phosphate pathway
Pentose and glucuronate interconversions
Phenylalanine metabolism
Tyrosine
ddc
Dopamine
Phenylalanine
Phenyl ethylamine
aoc2
Phenyl acetaldehyde
ddc
Valine catabolism
echs1hibch
Propionyl CoA
echs1
3-Hydroxy propionyl CoA
hibch
3-Hydroxypropionate
beta-Alanine metabolism
Spermidine
1,3-Diamino-propane
aldh16a1
β-Aminopropion-aldehyde
aoc2
β-Alanine
Malonic semialdehyde
Taurine
3-Sulfino-alanine
Cystein
Glutamate
Taurine and hypotaurine metabolism
N-Acetyl aspartate
Aspartate
Alanine
agxt2
pyruvate
Alanine, aspartate and glutamate metabolism
Irreversible reaction
Reversible reaction
Control
Low concentration
High concentration
* P<0.05
** P<0.005

Conclusion

In this study, the biological perturbation of metabolites and proteins was analyzed by GC-MS/MS and LC-MS/MS to identify the toxicological effect of PCP on zebrafish. The treatment concentrations of PCP were based on level of LC_{50}; control, low exposure group (1/10 LC_{50}) and high exposure group (LC_{50}). Using GC-MS/MS in MRM mode, 397 targeted metabolites in homogenized zebrafish samples were analyzed after TMS derivatization. As, a result, 180 metabolites were detected in zebrafish samples and 74 metabolic biomarkers were selected by VIP and ANOVA. These were chosen as metabolites that cause significant changes in zebrafish when exposed to PCP, and hierarchical heat map of the 74 biomarkers visually shows the biological perturbation. Using MetaboAnalyst 4.0, eight metabolic pathways were selected in the pathway analysis of biomarkers metabolites; pentose phosphate pathway, pentose and glucuronate interconversions, taurine and hypotaurine metabolism, glutamine and glutamate metabolism, alanine, aspartate and glutamate metabolism, β-alanine metabolism, ascorbate and aldarate metabolism and phenylalanine metabolism.

Label-free quantitative proteomics in zebrafish exposed to PCP were performed by LC-Orbitrap-MS/MS. Six individual samples from each of the two control and high exposure group were pooled and homogenized for proteomic approach. A 200 μg equivalent of protein extracted with phosphate buffer (0.1M, pH 7.4) were treated by FASP method, the in-solution trypsin digestion. After analysis of LC-Orbitrap-MS/MS, 2108 proteins were detected by data processing with PD 2.4 and 376 protein biomarkers were identified through volcano plot (fold change and p-value). Through integrative pathway analysis of metabolomic/proteomic biomarkers using MetaboAnalyst 4.0, seven metabolic pathways were selected for identification of toxicological effects of PCP in zebrafish; pentose phosphate pathway, pentose and glucuronate interconversions,

taurine and hypotaurine metabolism, β-alanine metabolism, ascorbate and aldarate metabolism, alanine, aspartate and glutamate metabolism, and phenylalanine metabolism.

These seven metabolic pathways were interpreted using KEGG map, and the toxicological damage that occurs when exposed to PCP and defense mechanisms to counteract it have been identified. The biochemical toxicity of PCP manifested itself as inhibition of ribose synthesis, accumulation of 3-HP & β-alanine, defect of *echs1 & hibch*, reduction of NAA & tyrosine. On the other hand, the corresponding defense mechanism appeared as an increase of taurine and glucuronic acid. Furthermore, ROS and MDA were assessed to evaluate the oxidative stress of PCP in zebrafish, and the oxidative toxicity of PCP was proved, resulting statistically increased the level of MDA. These results suggest toxicological tendency of significant perturbations in zebrafish by the exposure of PCP.

References

Akhmedov, M., Arribas, A., Montemanni, R., Bertoni, F., and Kwee, I. (2017). OmicsNet: Integration of Multi-Omics Data using Path Analysis in Multilayer Networks. bioRxiv, 238766.

Ali, F. E., Barnham, K. J., Barrow, C. J., and Separovic, F. (2004). Metal catalyzed oxidation of tyrosine residues by different oxidation systems of copper/hydrogen peroxide. Journal of inorganic biochemistry, 98(1), 173-184.

Basheer, C., Lee, H. K., and Tan, K. S. (2004). Endocrine disrupting alkylphenols and bisphenol-A in coastal waters and supermarket seafood from Singapore.

Bernotti, S., Seidman, E., Sinnett, D., Brunet, S., Dionne, S., Delvin, E et al. (2003). Inflammatory reaction without endogenous antioxidant response in Caco-2 cells exposed to iron/ascorbate-mediated lipid peroxidation. American Journal of Physiology-Gastrointestinal and Liver Physiology, 285(5), G898-G906.

Bernotti, S., Seidman, E., Sinnett, D., Brunet, S., Dionne, S., Delvin, E et al. (2003). Inflammatory reaction without endogenous antioxidant response in Caco-2 cells exposed to iron/ascorbate-mediated lipid peroxidation. American Journal of Physiology-Gastrointestinal and Liver Physiology, 285(5), G898-G906.

Bindels, L. B., Porporato, P., Dewulf, E. M., Verrax, J., Neyrinck, A. M., Martin, J. C et al. (2012). Gut microbiota-derived propionate reduces cancer cell proliferation in the liver. British journal of cancer, 107(8), 1337-1344.

Birken, D. L., and Oldendorf, W. H. (1989). N-acetyl-L-aspartic acid: a literature review of a compound prominent in 1H-NMR spectroscopic studies of brain. Neuroscience & Biobehavioral Reviews, 13(1), 23-31.

Brunet, S., Thibault, L., Lepage, G., Seidman, E. G., Dube, N., and Levy, E. (2000). Modulation of endoplasmic reticulum-bound cholesterol regulatory enzymes by iron/ascorbate-mediated lipid peroxidation. Free Radical Biology and Medicine, 28(1), 46-54.

Buffa, P., Carafoli, E., and Muscatello, U. (1963). Mitochondrial biochemical lesion and pyrogenic effect of pentachlorophenol. Biochemical Pharmacology, 12(8), 769-778.

Cao, M., Hou, Y., Zhang, E., Tu, S., and Xiong, S. (2019). Ascorbic acid induced activation of persulfate for pentachlorophenol degradation. Chemosphere, 229, 200-205.

Carson, P. E., Flanagan, C. L., Ickes, C. E., and Alving, A. S. (1956). Enzymatic deficiency in primaquine-sensitive erythrocytes. Science, 124(3220), 484-485.

Chen, X., Zhang, J., Wang, R., Liu, H., Bao, C., Wu, S et al. (2020). UPLC-Q-TOF/MS-Based Serum and Urine Metabonomics Study on the Ameliorative Effects of Palmatine on Helicobacter pylori–Induced Chronic Atrophic Gastritis. Frontiers in Pharmacology, 11.

Chong, J., Soufan, O., Li, C., Caraus, I., Li, S., Bourque, G et al. (2018). MetaboAnalyst 4.0: towards more transparent and integrative metabolomics analysis. Nucleic acids research, 46(W1), W486-W494.

Chun, A. Y., Yunxiao, L., Ashok, S., Seol, E., and Park, S. (2014). Elucidation of toxicity of organic acids inhibiting growth of Escherichia coli W. Biotechnology and bioprocess engineering, 19(5), 858-865.

Dai, Y. J., Jia, Y. F., Chen, N., Bian, W. P., Li, Q. K., Ma, Y. B et al. (2014). Zebrafish as a model system to study toxicology. Environmental toxicology and chemistry, 33(1), 11-17.

Das, J., Ghosh, J., Manna, P., Sinha, M., and Sil, P. C. (2009). Taurine protects rat testes against NaAsO2-induced oxidative stress and apoptosis via mitochondrial dependent and independent pathways. Toxicology letters, 187(3), 201-210.

Diz, A. P., Truebano, M., and Skibinski, D. O. (2009). The consequences of sample pooling in proteomics: an empirical study. Electrophoresis, 30(17), 2967-2975.

El Agouza, I. M., Eissa, S. S., El Houseini, M. M., El-Nashar, D. E., and Abd El Hameed, O. M. (2011). Taurine: a novel tumor marker for enhanced detection of breast cancer among female patients. Angiogenesis, 14(3), 321.

Ennis, H. L., and Lubin, M. (1964). Cycloheximide: aspects of inhibition of protein synthesis in mammalian cells. Science, 146(3650), 1474-1476.

EPA., (2008), "Environmental fate and transport assessment of pentachlorophenol (PCP) for Reregistration Eligibility Decision (RED) process." Washington (DC), USA: United States Environmental Protection Agency.

Ferdinandusse, S., Waterham, H. R., Heales, S. J., Brown, G. K., Hargreaves, I. P., Taanman, J. W et al. (2013). HIBCH mutations can cause Leigh-like disease with combined deficiency of multiple mitochondrial respiratory chain enzymes and pyruvate dehydrogenase. Orphanet journal of rare diseases, 8(1), 188.

Folkes, L. K., Trujillo, M., Bartesaghi, S., Radi, R., and Wardman, P. (2011). Kinetics of reduction of tyrosine phenoxyl radicals by glutathione. Archives of biochemistry and biophysics, 506(2), 242-249.

Fraser, D. L., Stander, B. A., and Steenkamp, V. (2019). Cytotoxic activity of pentachlorophenol and its active metabolites in SH-SY5Y neuroblastoma cells. Toxicology in Vitro, 58, 118-125.

Ge, J., Pan, J., Fei, Z., Wu, G., and Giesy, J. P. (2007). Concentrations of pentachlorophenol (PCP) in fish and shrimp in Jiangsu Province, China. Chemosphere, 69(1), 164-169.

Gemelli, T., de Andrade, R. B., Rojas, D. B., Bonorino, N. F., Mazzola, P. N., Tortorelli, L. S et al. (2013). Effects of β-alanine administration on selected parameters of oxidative stress and phosphoryltransfer network in cerebral cortex and cerebellum of rats. Molecular and cellular biochemistry, 380(1-2), 161-170.

Gene, O. C. (2015). Gene ontology consortium: going forward. Nucleic Acids Res, 43(Database issue), D1049-56.

Gunnarsson, L., Jauhiainen, A., Kristiansson, E., Nerman, O., and Larsson, D. J. (2008). Evolutionary conservation of human drug targets in organisms used for environmental risk assessments. Environmental science & technology, 42(15), 5807-5813.

Guo, C., Huang, X. Y., Yang, M. J., Wang, S., Ren, S. T., Li, H et al. (2014). GC/MS-based metabolomics approach to identify biomarkers differentiating survivals from death in crucian carps infected by Edwardsiella tarda. Fish & shellfish immunology, 39(2), 215-222.

Gupta, R., Min, C. W., Kramer, K., Agrawal, G. K., Rakwal, R., Park, K. H et al. (2018). A multi-omics analysis of glycine max leaves reveals alteration in flavonoid and isoflavonoid metabolism upon ethylene and abscisic acid treatment. Proteomics, 18(7), 1700366.

Ham, B. J., Chey, J., Yoon, S. J., Sung, Y., Jeong, D. U., Ju Kim, S et al. (2007). Decreased N-acetyl-aspartate levels in anterior cingulate and hippocampus in subjects with post-traumatic stress disorder: a proton magnetic resonance spectroscopy study. European journal of neuroscience, 25(1), 324-329.

Hasin, Y., Seldin, M., and Lusis, A. (2017). Multi-omics approaches to disease. Genome biology, 18(1), 1-15.

Hirata, Y., Kobayashi, T., Nishiumi, S., Yamanaka, K., Nakagawa, T., Fujigaki, S et al. (2017). Identification of highly sensitive biomarkers that can aid the early detection of pancreatic cancer using GC/MS/MS-based targeted metabolomics. Clinica Chimica Acta, 468, 98-104.

Hong, H. C., Zhou, H. Y., Luan, T. G., and Lan, C. Y. (2005). Residue of pentachlorophenol in freshwater sediments and human breast milk collected from the Pearl River Delta, China. Environment international, 31(5), 643-649.

IARC., (1991). A consensus report of an IARC Monographs Working Group on the Use of Mechanisms of Carcinogenesis in Risk Identification (IARC Intern Tech Rep No. 91/002).

Ibero-Baraibar, I., Romo-Hualde, A., Gonzalez-Navarro, C. J., Zulet, M. A., and Martinez, J. A. (2016). The urinary metabolomic profile following the intake of meals supplemented with a cocoa extract in middle-aged obese subjects. Food & function, 7(4), 1924-1931.

Iglewski, B. H., and Kabat, D. (1975). NAD-dependent inhibition of protein synthesis by Pseudomonas aeruginosa toxin. Proceedings of the National Academy of Sciences, 72(6), 2284-2288.

Khansari, N., Shakiba, Y., and Mahmoudi, M. (2009). Chronic inflammation and oxidative stress as a major cause of age-related diseases and cancer. Recent patents on inflammation & allergy drug discovery, 3(1), 73-80.

Kim, K., Kwon, O., Ryu, T. Y., Jung, C. R., Kim, J., Min, J. K et al. (2019). Propionate of a microbiota metabolite induces cell apoptosis and cell cycle arrest in lung cancer. Molecular medicine reports, 20(2), 1569-1574.

Krieger, R. (2010). Hayes' handbook of pesticide toxicology (Vol. 1). Academic press. p.629.

Krieger, R. (2010). Hayes' handbook of pesticide toxicology (Vol. 1). Academic press. p. 603

Kruger, N. J., and von Schaewen, A. (2003). The oxidative pentose phosphate pathway: structure and organisation. Current opinion in plant biology, 6(3), 236-246.

Kuehnbaum, N. L., and Britz-McKibbin, P. (2013). New advances in separation science for metabolomics: resolving chemical diversity in a post-genomic era. Chemical reviews, 113(4), 2437-2468.

Lascorz, J., Chen, B., Hemminki, K., and Försti, A. (2011). Consensus pathways implicated in prognosis of colorectal cancer identified through systematic enrichment analysis of gene expression profiling studies. PloS one, 6(4), e18867.

Lee, H. K., Kim, K., Lee, J., Lee, J., Lee, J., Kim, S et al. (2020). Targeted toxicometabolomics of endosulfan sulfate in adult zebrafish (Danio rerio) using GC-MS/MS in multiple reaction monitoring mode. Journal of Hazardous Materials, 389, 122056.

Li, J., Yang, L., Li, Y., Tian, Y., Li, S., Jiang, S et al. (2015). Metabolomics study on model rats of chronic obstructive pulmonary disease treated with Bu-Fei Jian-Pi. Molecular medicine reports, 11(2), 1324-1333.

Lin, S.-K., (2000), Agrochemicals: Composition, Production, Toxicology, Applications. Edited by Franz Müller. Molecular Diversity Preservation International. pp.578.

MacMullan, M. A., Dunn, Z. S., Graham, N., Yang, L., and Wang, P. (2019). Quantitative proteomics and metabolomics reveal biomarkers of disease as potential immunotherapy targets and indicators of therapeutic efficacy. Theranostics, 9(25), 7872.

Maheshwari, N., Khan, F. H., and Mahmood, R. (2019). Pentachlorophenol-induced cytotoxicity in human erythrocytes: enhanced generation of ROS and RNS, lowered antioxidant power, inhibition of glucose metabolism, and morphological changes. Environmental Science and Pollution Research, 26(13), 12985-13001.

Marti-Sanchez, L., Baide-Mairena, H., Marcé-Grau, A., Pons, R., Skouma, A., López-Laso, E et al. (2020). Delineating the neurological phenotype in children with defects in the ECHS1 or HIBCH gene. Journal of Inherited Metabolic Disease.

Mateos, R., Lecumberri, E., Ramos, S., Goya, L., and Bravo, L. (2005). Determination of malondialdehyde (MDA) by high-performance liquid chromatography in serum and liver as a biomarker for oxidative stress: Application to a rat model for hypercholesterolemia and

evaluation of the effect of diets rich in phenolic antioxidants from fruits. Journal of Chromatography B, 827(1), 76-82.

Mates, J. M., Segura, J. A., Alonso, F. J., and Marquez, J. (2012). Sulphur-containing non enzymatic antioxidants: therapeutic tools against cancer. Front Biosci (Schol Ed), 4, 722-748.

Matés, J. M., Segura, J. A., Alonso, F. J., and Márquez, J. (2012). Oxidative stress in apoptosis and cancer: an update. Archives of toxicology, 86(11), 1649-1665.

Matés, J. M., Segura, J. A., Alonso, F. J., and Márquez, J. (2012). Oxidative stress in apoptosis and cancer: an update. Archives of toxicology, 86(11), 1649-1665.

Matsubara, K., Mori, H., Hirai, N., Yasukawa, K., Honda, T., and Takanashi, J. I. (2016). Elevated taurine and glutamate in cerebral juvenile xanthogranuloma on MR spectroscopy. Brain and Development, 38(10), 964-967.

Meng, C., Kuster, B., Culhane, A. C., and Gholami, A. M. (2014). A multivariate approach to the integration of multi-omics datasets. BMC bioinformatics, 15(1), 162.

Michałowicz, J., Stufka-Olczyk, J., Milczarek, A., and Michniewicz, M. (2011). Analysis of annual fluctuations in the content of phenol, chlorophenols and their derivatives in chlorinated drinking waters. Environmental Science and Pollution Research, 18(7), 1174-1183.

Mishra, P., Gong, Z., and Kelly, B. C. (2017). Assessing biological effects of fluoxetine in developing zebrafish embryos using gas chromatography-mass spectrometry based metabolomics. Chemosphere, 188, 157-167.

Moffett, J. R., Arun, P., Ariyannur, P. S., and Namboodiri, A. M. (2013). N-Acetylaspartate reductions in brain injury: impact on post-injury neuroenergetics, lipid synthesis, and protein acetylation. Frontiers in neuroenergetics, 5, 11.

Müting, D., Kalk, J. F., Fischer, R., Wuzel, H., and Reikowski, J. (1988). Hepatic detoxification and hepatic function in chronic active hepatitis with and without cirrhosis. Digestive diseases and sciences, 33(1), 41-46.

Navas-Carrillo, D., Rodriguez, J. M., Montoro-García, S., and Orenes-Piñero, E. (2017). High-resolution proteomics and metabolomics in thyroid cancer: Deciphering novel biomarkers. Critical reviews in clinical laboratory sciences, 54(7-8), 446-457.

Nnodu, U., and Whalen, M. M. (2008). Pentachlorophenol decreases ATP levels in human natural killer cells. Journal of Applied Toxicology, 28(8), 1016-1020.

Peters, H., Buck, N., Wanders, R., Ruiter, J., Waterham, H., Koster, J et al. (2014). ECHS1 mutations in Leigh disease: a new inborn error of metabolism affecting valine metabolism. Brain, 137(11), 2903-2908.

Peters, H., Ferdinandusse, S., Ruiter, J. P., Wanders, R. J., Boneh, A., and Pitt, J. (2015). Metabolite studies in HIBCH and ECHS1 defects: Implications for screening. Molecular genetics and metabolism, 115(4), 168-173.

Peterson, R. T., and MacRae, C. A. (2012). Systematic approaches to toxicology in the zebrafish. Annual review of pharmacology and toxicology, 52, 433-453.

Ralser, M., Wamelink, M. M., Kowald, A., Gerisch, B., Heeren, G., Struys, E. A et al. (2007). Dynamic rerouting of the carbohydrate flux is key to counteracting oxidative stress. Journal of biology, 6(4), 10.

Ruhoy, I. S., and Saneto, R. P. (2014). The genetics of Leigh syndrome and its implications for clinical practice and risk management. The application of clinical genetics, 7, 221.

Schuff, N., Neylan, T. C., Lenoci, M. A., Du, A. T., Weiss, D. S., Marmar, C. R et al. (2001). Decreased hippocampal N-acetylaspartate in the absence of atrophy in posttraumatic stress disorder. Biological psychiatry, 50(12), 952-959.

Shan, X., Chang, Y., and Glenn Lin, C. L. (2007). Messenger RNA oxidation is an early event preceding cell death and causes reduced protein expression. The FASEB Journal, 21(11), 2753-2764.

Shetewy, A., Shimada-Takaura, K., Warner, D., Jong, C. J., Al Mehdi, A. B., Alexeyev, M et al. (2016). Mitochondrial defects associated with β-alanine toxicity: relevance to hyper-beta-alaninemia. Molecular and cellular biochemistry, 416(1-2), 11-22.

Song, Y. N., Dong, S., Wei, B., Liu, P., Zhang, Y. Y., and Su, S. B. (2017). Metabolomic mechanisms of gypenoside against liver fibrosis in rats: An integrative analysis of proteomics and metabolomics data. PLoS One, 12(3), e0173598.

Stincone, A., Prigione, A., Cramer, T., Wamelink, M. M., Campbell, K., Cheung, E et al. (2015). The return of metabolism: biochemistry and physiology of the pentose phosphate pathway. Biological Reviews, 90(3), 927-963.

Sun, H., Zhang, A. H., Song, Q., Fang, H., Liu, X. Y., Su, J et al. (2018). Functional metabolomics discover pentose and glucuronate interconversion pathways as promising targets for Yang Huang syndrome treatment with Yinchenhao Tang. RSC advances, 8(64), 36831-36839.

Thilmann, R., Xie, Y., Kleihues, P., and Kiessling, M. (1986). Persistent inhibition of protein synthesis precedes delayed neuronal death in postischemic gerbil hippocampus. Acta neuropathologica, 71(1), 88-93.

Trygg, J., Holmes, E., and Lundstedt, T. (2007). Chemometrics in metabonomics. Journal of proteome research, 6(2), 469-479.

Tsugawa, H., Tsujimoto, Y., Sugitate, K., Sakui, N., Nishiumi, S., Bamba, T et al. (2014). Highly sensitive and selective analysis of widely targeted metabolomics using gas chromatography/triple-quadrupole mass spectrometry. Journal of bioscience and bioengineering, 117(1), 122-128.

Ueno, Y., Nakajima, M., Sakai, K., Ishii, K., Sato, N., and SHIMADA, N. (1973). Comparative toxicology of trichothec mycotoxins: inhibition of protein synthesis in animal cells. The Journal of Biochemistry, 74(2), 285-296.

Umemura, T., Kuroiwa, Y., Kitamura, Y., Ishii, Y., Kanki, K., Kodama, Y et al. (2006). A crucial role of Nrf2 in in vivo defense against oxidative damage by an environmental pollutant, pentachlorophenol. Toxicological Sciences, 90(1), 111-119.

United Nations., (2010) Exploration of management options por pentachlorophenol (PCP). Paper for the 8th meeting of the UNECE CLRTAP Task Force on Persistent Organic Pollutants, Montreal, 18–20 May.

Villar, M., Ayllón, N., Alberdi, P., Moreno, A., Moreno, M., Tobes, R. et al. (2015). Integrated metabolomics, transcriptomics and proteomics identifies metabolic pathways affected by Anaplasma phagocytophilum infection in tick cells. Molecular & Cellular Proteomics, 14(12), 3154-3172.

Wang, W., Li, Z., Gan, L., Fan, H.,and Guo, Y. (2018). Dietary supplemental Kluyveromyces marxianus alters the serum metabolite profile in broiler chickens. Food & function, 9(7), 3776-3787.

Ward, M. H., Colt, J. S., Metayer, C., Gunier, R. B., Lubin, J., Crouse, V et al. (2009). Residential exposure to polychlorinated biphenyls and organochlorine pesticides and risk of childhood leukemia. Environmental health perspectives, 117(6), 1007-1013.

Ware, G. W., (2000), *The pesticide book*. Thomson Publications. pp. 86,160

Warnecke, T. E., Lynch, M. D., Karimpour-Fard, A., Lipscomb, M. L., Handke, P., Mills, T et al. (2010). Rapid dissection of a complex phenotype through genomic-scale mapping of fitness altering genes. Metabolic engineering, 12(3), 241-250.

Warnecke, T., and Gill, R. T. (2005). Organic acid toxicity, tolerance, and production in Escherichia coli biorefining applications. Microbial cell factories, 4(1), 1-8.

Whitley, L. S., and Sikora, R. A. (1970). The effect of three common pollutants on the respiration rate of tubificid worms. Journal (Water Pollution Control Federation), R57-R66.

Wiśniewski, J. R., Zougman, A., Nagaraj, N., and Mann, M. (2009). Universal sample preparation method for proteome analysis. Nature methods, 6(5), 359-362.

Xia, J., and Wishart, D. S. (2010). MSEA: a web-based tool to identify biologically meaningful patterns in quantitative metabolomic data. Nucleic acids research, 38(suppl_2), W71-W77.

Xie, Z. C., Li, T. T., Gan, B. L., Gao, X., Gao, L., Chen, G et al. (2018). Investigation of miR-136-5p key target genes and pathways in lung squamous cell cancer based on TCGA database and bioinformatics analysis. Pathology-Research and Practice, 214(5), 644-654.

Xie, Z. C., Li, T. T., Gan, B. L., Gao, X., Gao, L., Chen, G et al. (2018). Investigation of miR-136-5p key target genes and pathways in lung squamous cell cancer based on TCGA database and bioinformatics analysis. Pathology-Research and Practice, 214(5), 644-654.

Yao, W., Zhang, L., Hua, Y., Ji, P., Li, P., Li, J et al. (2015). The investigation of anti-inflammatory activity of volatile oil of Angelica sinensis by plasma metabolomics approach. International immunopharmacology, 29(2), 269-277.

Yates III, J. R. (2011). A century of mass spectrometry: from atoms to proteomes. nature methods, 8(8), 633-637.

Yin, D., Gu, Y., Li, Y., Wang, X., and Zhao, Q. (2006). Pentachlorophenol treatment in vivo elevates point mutation rate in zebrafish p53 gene. Mutation Research/Genetic Toxicology and Environmental Mutagenesis, 609(1), 92-101.

Zaitsu, K., and Hayashi, Y. (2019). GC/MS/MS-based targeted metabolomics for pathophysiological analysis of animal models. Medical Mass Spectrometry (Web), 3(1).

Zaitsu, K., Noda, S., Iguchi, A., Hayashi, Y., Ohara, T., Kimura, Y et al. (2018). Metabolome analysis of the serotonin syndrome rat model: Abnormal muscular contraction is related to metabolic alterations and hyper-thermogenesis. Life sciences, 207, 550-561.

Zamboni, N., Saghatelian, A., and Patti, G. J. (2015). Defining the metabolome: size, flux, and regulation. Molecular cell, 58(4), 699-706.

Zhang, B., Kirov, S., and Snoddy, J. (2005). WebGestalt: an integrated system for exploring gene sets in various biological contexts. Nucleic acids research, 33(suppl_2), W741-W748.

Zhang, X., Tu, S., Wang, Y., Xu, B., and Wan, F. (2014). Mechanism of taurine-induced apoptosis in human colon cancer cells. Acta Biochim Biophys Sin, 46(4), 261-272.

Zheng, W., Yu, H., Wang, X., and Qu, W. (2012). Systematic review of pentachlorophenol occurrence in the environment and in humans in China: not a negligible health risk due to the re-emergence of schistosomiasis. Environment international, 42, 105-116.

Zhou, Y., Yang, K., Zhang, D., Duan, H., Liu, Y., and Guo, M. (2018). Metabolite accumulation and metabolic network in developing roots of Rehmannia glutinosa reveals its root developmental mechanism and quality. Scientific reports, 8(1), 1-11.

초 록

서울대학교 대학원

농생명공학부 응용생명화학전공

한희주

Pentachlorophenol (PCP)는 살충제나 나무 보존제의 용도로 사용되어왔고 발암가능성 2B 등급으로 지정된 물질이다. PCP는 그 구조상 화학적인 안정성을 지녀 쉽게 분해되지 않아 환경에서 잔류할 확률이 높다. 이러한 PCP의 특성상, 환경 잔류를 통해 수중 생태계에 노출될 수 있어 이번 연구에서는 GC-MS/MS를 이용한 표적 대사체학 방법와 LC-Orbitrap-MS/MS을 통한 단백질체학 방법를 연계함으로써 zebrafish 성체 내에서의 독성 메커니즘을 규명해보고자 하였다. 48시간동안 3그룹의 zebrafish는 PCP에 각각 0, 1/10 LC_{50}, LC_{50} 수준으로 노출되었다. GC-MS/MS의 multiple reaction monitoring (MRM) mode를 통하여 총 397개의 대사체가 분석되었고 그중 180 성분이 확인되었다. SIMCA+와 Metaboanalyst 프로그램을 활용하여 통계적인 분석을 수행하였다. 3 그룹은 principal component analysis (PCA)와 partial least squares-discriminant analysis (PLS-DA), 2 모델에서 통계적으로 유의미하게 분리되는 것을 확인할 수 있었다. 180 성분 중 variable importance in the projection (VIP) 과 analysis of variance (ANOVA) tests 를 통해서 총 74종의 대사체 바이오마커를 선정하였고 heatmap을 구성하였다. PCP에 의한 산화적 스트레스

는 MDA와 ROS assay를 통해서 확인되었다. 대사체를 통해서는 독성학적으로 교란된 총 8가지의 대사경로 확인할 수 있었다. 이 후, control과 high exposure group에 한하여 단백질체학을 진행하여 총 2108개의 단백질이 검출되었다. 그중 fold change와 p-value를 통해서 376개의 바이오마커를 선정하였다. 단백질 바이오마커의 기능적인 분류에 따른 단백질을 확인하고자 gene ontology analysis를 수행하였다. 이후 대사체학/단백질체학의 바이오마커를 통합하여 integrative metabolic pathways를 도출한 결과 총 7가지의 유의미한 pathway를 확인하였다: pentose phosphate pathway, pentose and glucuronate pathway, phenylalanine metabolism, ascorbate and aldarate metabolism, taurine and hypotaurine metabolism, alanine, asparatate and glutamate metbaolism and β-alanine metabolism. PCP에 노출되었을 때 이러한 대사체학과 단백질체학의 연계 대사경로상의 변화는 독성학적으로 유의미한 효과와 방어기작의 활성을 나타내는 결과를 초래한 것으로 확인된다.

주요어 : Pentachlorophenol, 대사, 대사체학, 단백질체학, LC-Orbitrap-MS/MS, GC-MS/MS, 제브라피쉬

학 번 : 2019-23867

Acknowledgements

이번 학위논문을 작성하는데까지 많은 분들의 도움과 관심이 있었기에 이 글을 통해 감사인사를 드리려고 합니다.

무엇보다도 저에게 의미있는 연구를 진행할 수 있게 해주시고 선택의 기로에 있을 때 스스로 생각할 수 있도록 이정표가 되어주신 김정한 교수님께 감사드립니다. 제가 한단계 더 성장할 수 있도록 이끌어주셨던 교수님의 가르침을 기반으로 앞으로의 삶에서도 발전적인 사람이 될 수 있도록 노력하며 정진하겠습니다. 연구부터 논문 작성까지 많은 도움을 주셨던 이화경 교수님 바쁘신 와중에도 자기 일처럼 신경써서 도와주시고 어떤 질문이라도 친절하고 상세히 대답해주셔서 감사드립니다. 또한 학부 새내기때부터 석사과정 마칠 때까지 많은 가르침과 조언을 주신 김민균 교수님, 김수언 교수님, 권용훈 교수님, 노희명 교수님, 이상기 교수님, 오기봉 교수님, 배의영 교수님, 신찬석 교수님, 최양도 교수님께도 진심으로 감사드립니다.

학부 졸업실험하면서 분석기기에 관심이 생겨서 석사로 진학하고 졸업하는데까지 많은 배움을 주었던 저희 실험실 사람들에게도 감사드립니다. 어떤 돌발 상황에서도 침착함을 유지할 수 있도록 해준 기기마스터 정학 선배, 티격태격하면서도 기본적인 것부터 하나하나 가르쳐주고 항상 아껴줬던 제 사수인 락도 오빠 감사해요. 2년 생활하는

동안 실험실 분위기메이커였던 은영언니와 저 항상 예뻐라해줬던 막학기 옆짝궁 원수 오빠도 정말 감사해요. 그리고 실험실 마지막 막내라 서로 많이 의지했던 보은언니, 언니가 동기여서 좋았어요. 첫 학회에서 실험실 막내라며 챙겨주고 고민 상담도 잘 해줘서 닮고 싶었던 지호 오빠, 한 학기동안 함께 필드 실험도 가고 비슷해서 신기했던 용호 선배도 감사드려요. 짧은 시간동안 저한테 키다리 아저씨 같았던 강헌선배도 감사해요. 그리고 석사 초에 적응할 수 있게 옆에서 많이 아껴준 아름 언니, 서현 언니, 진이 언니, 상율 오빠 장난꾸러기 동생 예뻐해줘서 고마워요.

석사 하는 동안 실험실 밖에서 숨통 트여준 학부 때 인연들에게도 너무 감사드립니다. 힘들어 할 때마다 계단에 앉아서 위로해주고 가끔 수다떨면서 활력을 불러넣어준 계단메이트 새연이랑 광웅오빠 진짜 너무 고마웠어. 그리고 2년차에 바통터치 받고 취업이랑 졸업에 치여서 힘들어했을 때 옆에서 달달한 거 먹여준 예진이랑 혜원이도 내가 많이 아낀다~

마지막으로 나의 든든한 버팀목인 가장 사랑하는 우리 가족들 너무 감사해요. 항상 자랑스러운 딸이 되려고 노력해왔는데 사실 그럴 수 있었던 이유는 어떤 상황에서도 나를 전적으로 지지해주는 가족이 있었기 때문임을 밖에 나와 생활하면서 퇴근길에 전화하다 문득

깨달았어요. 상황을 털어놓고 현명한 행동을 할 수 있도록 고민상담해준 우리 아빠 아무리 힘들어도 제가 힘들다는 한마디에 데리러 달려와주는 거 알아요 감사해요. 그리고 엄마 제가 좋은 일이 있거나 나쁜 일이 있을 때 마치 자기 일인거 마냥 나보다 더 행복해하고 슬퍼해줘서 고마워요 그래서 나는 항상 중심을 잡고 서있을 수 있었어요. 나랑 참 비슷하면서도 다른 우리 오빠 무뚝뚝해서 연락도 잘 안하면서 나 집에 가는 날이면 다른 거 제쳐두고 가족이랑 함께 해줘서 고마워. 그리고 진짜 마지막으로 항상 늦은 시간에도 길 위험하다고 내 전화 기다려준 내 동생 희나야 내 인생에 가장 감사한 일은 너랑 쌍둥이라는거야 하고 싶은 말 너무 많지만 나중에 말로 할게 사랑해.

다시 한번 많은 분들께 감사드립니다. 지난 2년동안 인생에서 정말 많이 웃고 울고 많이 배우고 많이 느끼면서 거의 대부분의 시간을 실험실에서 보냈는데 돌이켜보니 그런 순간들이 있었기에 지금의 제가 있을 수 있음을 느낍니다. 항상 하나라도 더 배우겠다는 자세로 더 나은 사람이 될 수 있도록 노력하겠습니다. 감사합니다.